UNIVERSITY OF TWENTE.

Advanced Organ bioengineering and Therapeutics
Engineered Therapeutics (AOT-ET)

Active targeting of the extracellular matrix in the tumor microenvironment using novel collagen-binding peptides

Devin Veerman
s1726935

MSc Biomedical Engineering
January 28, 2022

Chairman
Prof. Dr. J. Prakash

Supervisors
Prof. Dr. J. Prakash
A.M.R.H. Mostafa, MSc

External members
Prof. Dr. H.B.J. Karperien
Dr.ir. J. Rouwkema

MSc Biomedical Engineering
Faculty of Science and Technology
University of Twente
P.O. Box 217
7500 AE Enschede
The Netherlands

Abstract

Cancer, or malignant tumor, is the second leading cause of death worldwide. During tumor progression, cancer cells actively act on and restructure their surrounding tissue, creating what is known as the tumor stroma or tumor microenvironment (TME). The TME supports tumors to survive, progress and become resistant to therapies.
Adenocarcinomas, such as pancreatic ductal adenocarcinoma (PDAC), are known for its high degree of desmoplasia resulting in the increased deposition of extracellular matrix (ECM) which is mainly comprised of collagens type I and III. Moreover, the increase in collagen type III appears to be more tumor-specific as compared to collagen type I.
Collagen as a therapeutic target to deliver therapeutic agents to the fibrotic TME is a promising but rarely investigated strategy. While most researchers focus on targeting collagen type I, targeting collagen type III is a novel approach to target desmoplastic tumors.
In this thesis, a novel collagen-binding peptide (CN3) was utilized and subjected to enzyme-linked immunosorbent assays (ELISAs) to evaluate binding affinity to various proteins of the ECM. Then, *in vitro* and *ex vivo* experiments were conducted to visualize binding of the peptide using collagen-producing cells, and murine PDAC models, respectively. Thereafter, the peptide was conjugated to liposomes to establish collagen-targeted nanocarriers. Liposomes were characterized, evaluated for binding affinity, and used for uptake experiments.
We found that first, the CN3-peptide showed increased binding affinity to collagen type III as compared to collagen type I. Furthermore, *in vitro* and *ex vivo* studies revealed colocalization of the CN3-peptide with cell-produced collagen. Yet, the CN3-peptide showed unspecific binding which might be related to its properties.
Next, the CN3-peptide could be coupled to the liposomes and showed increased binding affinity to both collagen types I and III as compared to the control. Uptake studies did not reveal a difference between between CN3-liposomes and control liposomes. Yet, data showed that the uptake studies were far from optimized.
In conclusion, we developed novel collagen-binding nanoparticles that could be used to target desmoplastic tumors. Further studies should focus on improving peptides' properties and binding specificity and evaluate the nanocarriers in more advanced models.

Contents

List of Figures

List of Tables

1 Introduction

1.1 Cancer and the tumor microenvironment

Cancer, or malignant tumor, is the second leading cause of death worldwide. Based on data from the Global Cancer Observatory (GCO), an estimated 19.3 million people were diagnosed with cancer and roughly 10 million cancer-related deaths were reported in 2020 [2].
In men, lung cancer, prostate cancer, and colorectal cancer were found to be most common cancers. Cancers of the lung, stomach, liver, esophagus, brain, and the pancreas appeared to be the most lethal cancers. Most deaths reside from lung cancer, colorectal cancer, stomach cancer, and liver cancer [2]. For women, breast cancer, colorectal cancer, and lung cancer were the most common diagnosed cancers in 2020. Cancers of the cervix uteri, colon, lung, ovary, stomach, liver, blood, esophagus, brain, and pancreas were found to be the most lethal types of cancers. Most deaths reside from breast cancer and lung cancer [2]. Due to declines in smoking, improved diagnostic and treatment modalities, the overall incidence and fatality rates are reducing since the 1990s. Still, the lifetime probability of being diagnosed with cancer is roughly 40% for men and 39% for women [3]. Following a projection that only takes growth and aging of the population into account, the predicted new cancer cases will be 28.4 million in 2040 [2]. The incidence rates and the predicted new cancer cases, indicate that cancer is still a major health problem.

Cancer is a multi-staged disease that is depicted by abnormal cell growth and proliferation [4, 5]. Hallmarks of cancer include: 1) sustaining proliferative signaling, 2) evading growth suppressors, 3) activating invasion and metastasis, 4) enabling replicative immortality, 5) inducing angiogenesis, and 6) resisting cell death [4]. Mutations in so-called tumor-suppressor genes and proto-oncogenes, which are usually genes that control proliferation and the cell cycle, generally lead to cancer. Recessive mutations in tumor-suppressor genes are characterized by a loss of functionally active tumor-suppressing proteins [4]. On the other hand, mutations in proto-oncogenes are dominant. Mutated proto-oncogenes become oncogenes and exhibit increased production of certain proteins that lead to over-stimulation of certain cell processes which, in its case, leads to the development of cancer [6, 7].

In recent years, the focus in cancer research has been shifted from the individual tumor cells towards the immediate environment surrounding the tumor cells. It has been found that during tumor progression, cancer cells actively act on and restructure their surrounding tissue, creating what is known as the tumor stroma or tumor microenvironment (TME) [8]. The TME supports tumors to survive, progress and become resistant to therapies [9, 10, 11]. In general, each tumor type has its own unique TME, including specific nonmalignant cells and extracellular matrix (ECM) proteins. Furthermore, the TME composition and structure can vary drastically from patient to patient, which makes a general description or classification of the TME difficult, however, certain characteristics of a TME can be shared among tumors. For instance, fibrotic tumors such as pancreatic ductal adenocarcinoma (PDAC), breast cancer, and lung cancer share common features in their TME such as an abundance of cancer-associated fibroblasts (CAFs) or the presence of desmoplasia, the overproduction of ECM proteins [12, 13, 14]. In figure 1, a schematic overview of the TME in fibrotic tumors is presented.

1.2 The extracellular matrix and cancer-associated fibroblasts

Shortly after the discovery of the TME and its role in cancer progression, the ECM, as the part of the TME, was initially discussed the least. However, many articles were published over the last decade that explained the role of the ECM in tumors [11].
In the early days, Dvorak *et al.* described tumors as 'wounds that do not heal' and evidence was presented that the

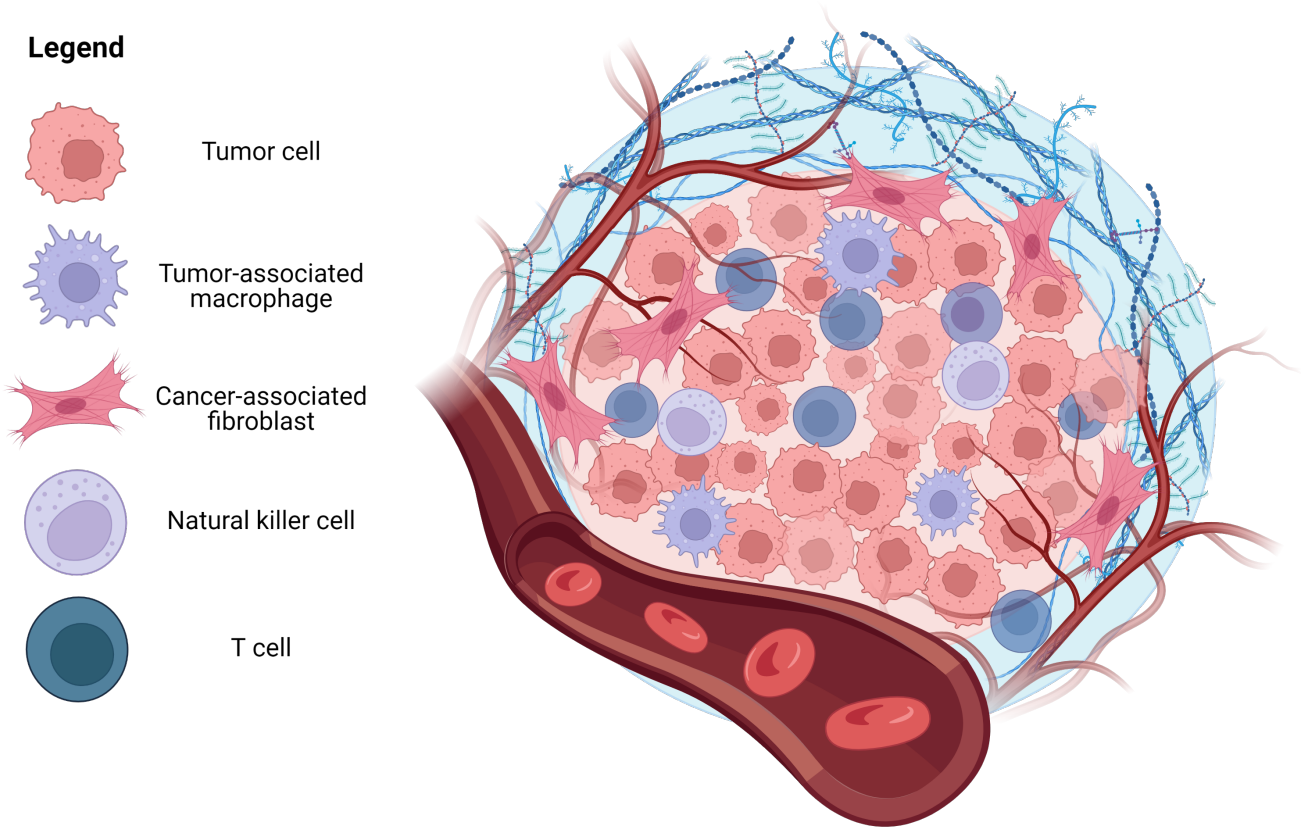

Figure 1: Schematic representation of the tumor microenvironment (TME) including different nonmalignant cellular components surrounded by extracellular matrix (ECM) created with BioRender.com.

progression of the tumor and its stroma are induced by the activation of the host's wound-healing response. However, this wound-healing response in tumors is continuously activated and seems to have much in common with the onset and progression of fibrosis [15]. Now, it has become clear that certain cells within the fibrotic TME are responsible for an excessive production of ECM molecules after chronic inflammation in a similar mechanism that drives tissue fibrosis [16, 17, 18]. ECM molecules, such as collagen, fibronectin, elastin, and laminin, can comprise up to 70% of the fibrotic TME. The creation of a hypoxic environment is a key feature of an abundant ECM within the fibrotic TME. As tumor cells have greater survival as compared to normal cells, a hypoxic environment favors proliferation of tumor cells [9].

While ECM-molecules are also produced by tumor cells themselves [11], most of the ECM is produced by cancer-associated fibroblasts (CAFs) [19, 20]. CAFs are spindle-shaped cells which are one of the most dominant components within the fibrotic TME. In the recent years, several growth factors and cytokines have been identified that can cause the activation of fibroblasts into a cancer-promoting or cancer-associated state, hence the name CAFs, as depicted in figure 2 [1]. CAFs are, as compared to normal fibroblasts, perpetually activated, and do not undergo apoptosis. The role of CAFs depends on their subtypes which has been thoroughly investigated in recent years [21, 22]. The CAF-population can roughly be divided into three subtypes, namely 1) myofibroblastic CAFs (myCAFs), 2) inflammatory CAFs (iCAFs), and 3) antigen-presenting CAFs (apCAFs) [22]. MyCAFs are known to build up and remodel the ECM structure while iCAFs are characterized by an immunomodulating secretome [22, 21, 23]. ApCAFs, as the name suggests, are able to present antigens to immune cells which can trigger an immune response [22]. By producing and maintaining the optimal environment for the tumor, these cells play a crucial role in the progression and survival of the tumor [24].

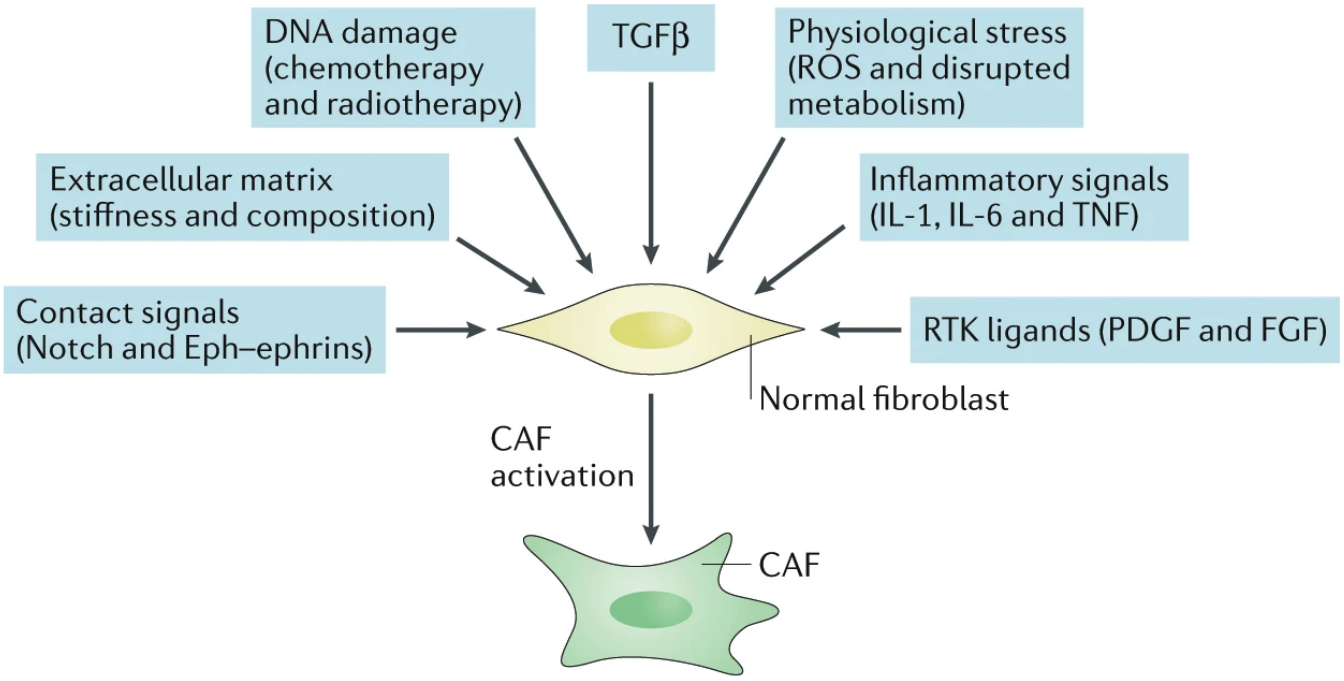

Figure 2: Schematic representation of different stimuli that can drive CAF activation [1].

1.3 Collagen as part of the extracellular matrix

Collagen is the major component of the ECM in fibrotic tumors [25, 26]. There are currently 28 identified types of collagens which are numbered with Roman numerals and are classified into four subfamilies, namely: i) fibril-forming collagens (I-III, V, XI, XXIV, XXVII), (ii) fibril-associated collagens (IX, XII, XIV, XVI, XIX, XX-XXII), (iii) network-forming collagens (IV, VIII, X), and (iv) membrane-anchored collagens (XIII, XVII, XXIII, XXV) [27]. Among all these types of collagens, collagen type I comprises 90% of the total collagen content in the human body [28].

Focusing on the fibrillar collagens, collagen type I is found in many tissues and is the main type of collagen in the human body [29]. Collagen type II is the main component of the cartilage matrix while collagen type III is usually found in soft tissues, tissues that need to withstand stretching, and near collagen type I [29, 30]. In addition, collagen type III is present during early stages of the wound healing process and, since this type of collagen is less rigid as compared to collagen type I, collagen type III is often regarded as immature and weak [31]. At later stages of wound healing, collagen type III is usually replaced by collagen type I [31, 32]. Fibril-forming collagens type I, III, and V are mainly produced by (activated) fibroblasts, like myCAFs during remodeling of the fibrotic TME [33, 34]. Therefore, the main types of collagens found in the ECM of the fibrotic TME are fibrillar collagens [25]. Fibrillar collagen is a large, right-handed helix glycoprotein that consists of three α-chains [35]. This set of α-chains can be homologous or heterogenous. In collagen type II and III, the α-chains are homologous which means that these collagens consist of three identical chains (e.g., three α1(II) chains for collagen type II) while in collagen type I, which is heterogenous, the protein consists of two α1(I) chains and one α2(I) chain [36]. The amino acid sequence of the α-chains in all types of collagens are characterized by X-Y-Glycine repeats where X and Y can be any amino acid [37]. In most cases, the X- and Y-position in the sequence is filled up by proline and hydroxyproline, respectively. Indeed, the proline-hydroxyproline-glycine sequence is the most common triplet in collagen [38]. The high content of proline and hydroxyproline facilitate hydrogen bond-formation between the α-chains while glycine stabilizes the protein [27]. The name of the α-chains is given according to their genes encoding for the particular type of collagen (e.g., COL1A1, COL1A2, COL3A1) [27]. These genes are transcribed followed by translation into a polypeptide in the rough endoplasmic reticulum (rER).

Several enzymes and molecular chaperones are required to facilitate post-translation modification (PTM) to form and process procollagen, including heat shock protein 47 (HSP47), prolyl-hydroxylase, and protein disulfide isomerase [39]. During PTM, one major step is the addition of hydroxyl groups to the lysine and proline residues which is facilitated by cofactor vitamin C [40]. The hydroxylated and glycosylated procollagen chains assemble into a triple helix in which three left-handed helices form a right-handed coil. In the extracellular space, tropocollagen is formed by removing the loose termini of procollagen [41]. Then, tropocollagen, which is also known as mature collagen, will spontaneously form collagen fibrils. Fibrils can form into mature collagen fibers by covalent linking of hydroxylysine and lysine by the lysyl oxidase (LOX) enzyme [42, 43, 44]. The process of collagen synthesis is schematically depicted in figure 3.

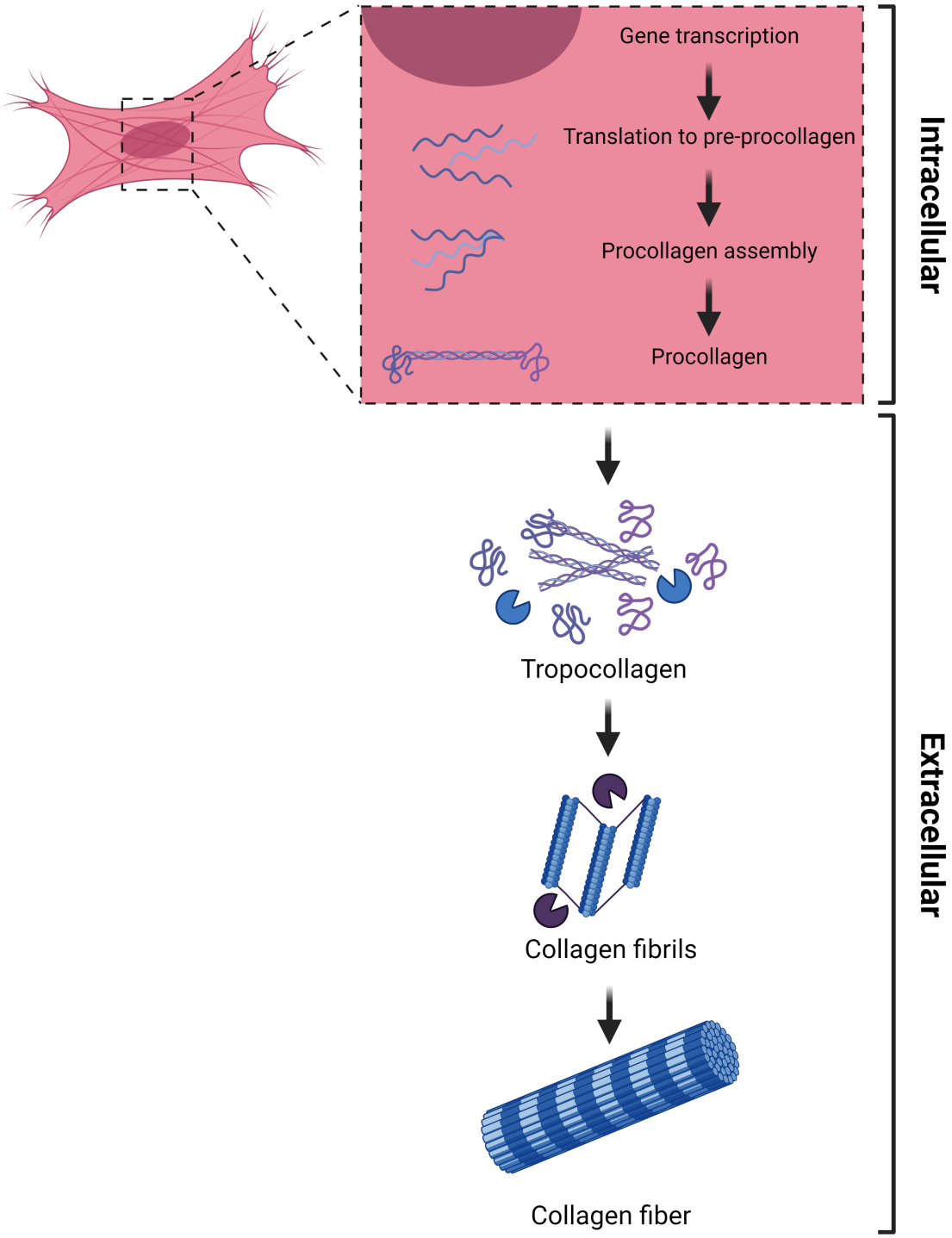

Figure 3: Schematic overview of the complexity of collagen synthesis created with BioRender.com. Collagen synthesis requires intracellular events as well as extracellular events.

1.4 Collagen in cancer

Collagen is known to provide structural support in the ECM. In healthy tissues, remodeling of the collagen helps to maintain tissue integrity and function. Remodeling is depicted by new collagens being synthesized and older proteins being degraded by metalloproteinases (MMPs) [45]. In cancer, myCAFs produce collagens uncontrollably, resulting in a dense network of collagen. A dense network of collagen may result in limited drug diffusion towards the tumor cells, and a reduced oxygen and nutrient supply. Reduced oxygen supply can result in hypoxia within tumors, inhibition of cytotoxic stress response, and induction of a process called epithelial-to-mesenchymal transition which is known to increase the number of ECM-producing cells [46, 11, 47]. Overexpression of certain collagens in certain types of cancers can be a hallmark of the disease. Many studies have shown a significant upregulation of collagen type I and type III in adenocarcinomas, which is a type of cancer that starts in the glands of various organs. As an example, Tian *et al.* found that 90% of the ECM in pancreatic ductal adenocarcinoma (PDAC) predominantly consisted of collagen types I and III [25]. Although collagen type III is less abundant as compared to collagen type I, the increase in collagen type III expression is a unique feature of many adenocarcinomas, including PDAC, breast cancer, colon cancer, and more [48, 49, 50].

1.5 Collagen as a target in the tumor microenvironment

Targeting and modulating myCAFs seems to be the best strategy to decrease the stromal density found in the fibrotic TME [51]. However, the population of CAFs within the TME has a high level of heterogeneity. This heterogeneity of the CAFs is expressed in multiple cell markers (e.g., α-SMA, FAP, FSP-1) that can define the entire CAF population. However, due to overlap in cell markers, there is no single marker that can distinguish one type of CAF from all other CAFs which makes it difficult to find a specific receptor [52]. In addition, the markers expressed in the CAF population varies among cancers which makes the process of selecting a target even more difficult [53, 54]. Therefore, instead of targeting markers on the collagen-producing cells (e.g., myCAFs), direct targeting of the produced collagen might be an effective way to deliver any therapeutic agent, which could have its effect on various types of cells, to the fibrotic TME. Moreover, the fact that collagen types I and III are overexpressed in all adenocarcinomas, targeting these types of collagens could aid in the development of the desired universal anti-cancer therapy for aggressive types of cancers.

Collagens in the fibrotic TME are exposed to the bloodstream due to the hyperpermeability of the tumor vasculature, a common feature in cancers [55]. By using the so-called enhanced permeability and retention (EPR) effect, collagen-binding moieties can enter the fibrotic TME in a passive manner [55]. Once entered, collagen-binding moieties can actively target the collagen in the fibrotic TME [55]. The most obvious strategy to realize targeting of collagen, is to use antibodies against collagen. Although antibodies have a high affinity towards its specific antigen, they do come with certain problems, including limited stability *in vivo*, high costs, a high molecular weight and its high affinity which might cause limited penetration into the targeted area [56, 57]. Therefore, using a molecule with a low molecular weight and moderate binding affinity is preferred. Here, peptides which are small, can have a moderate binding affinity, are comparably cheap, and can be chemically synthesized might come into play [58]. Peptides can be designed to bind to various molecules by utilizing non-covalent binding, such as forming hydrogen-bonds and binding through electrostatic interactions [59].

1.6 State-of-the-art

Literature on collagen-binding peptides has shown many applications to deliver therapeutics to or to diagnose, for instance, cartilage-defects by targeting collagen type II [60, 61, 62]. Only few have used these types of peptides to target the fibrotic TME by creating or using a peptide that has affinity towards collagen type I and/or collagen type III. Jeffrey A. Hubbell and co-workers conjugated many proteins and therapeutic agents to the collagen-binding domain of the von Willebrand factor. The A3-domain of the von Willebrand factor has a length of 186 amino acids, a molecular weight of 39.9 kDa, and shows high affinity against collagen types I and III [63, 64]. The same group also conjugated the collagen-binding domain to interleukin-2 [65], interleukin-12 [66], and to serum albumin which was conjugated to doxorubicin [67]. In all cases, the therapeutic agent displayed increased therapeutic efficacy and, in certain cases, less toxicity as compared to non-targeted therapeutic agents. A few years ago, Liang and colleagues conjugated an antibody-fragment to a small collagen-binding peptide. The collagen-binding antibody-fragment showed higher binding affinity to collagen type I as compared to the antibody-fragment without the collagen-binding peptide. Although, there was not an improvement in the therapeutic efficacy, Liang and colleagues did observe a longer retention time within tumors [68]. More recently, Deng and coworkers conjugated another small collagen type I-binding peptide to polymeric "nanoscavengers", a type of polymeric nanoparticles, and showed high accumulation in the ECM in various murine tumor models [69]. All these studies demonstrate that targeting collagen in the ECM of fibrotic tumors could be a good strategy to develop a universal therapy against tumors with dense stromal networks.

To date, using small peptides that favours binding to collagen type III, is a field that has not been discovered. As stated in section 1.4, this type of collagen is abundantly expressed in the fibrotic TME and seems more tumor-specific as compared to collagen type I. Therefore, aiming for collagen type III might increase specificity to fibrotic tumors.

1.7 Goal of the project

In this project, collagen-binding nanoparticles will be prepared and evaluated. Using a novel collagen-binding peptide, which will be named CN3 throughout the rest of the report, nanoparticles will be able to bind to the collagen within the fibrotic TME. The CN3-peptide is derived from the collagen-binding domain of the mannose receptor found mainly on macrophages [70]. The CN3-peptide has been studied previously within the group. Previous research focused mainly on the intracellular uptake of collagen types I and III by CAFs, and whether the uptake of the CN3-peptide is enhanced when bound to collagen type III as compared to collagen type I. Although the peptide seems to show increased binding to collagen type III, the binding affinity of the peptide to collagen types I and III was not evaluated in previous work.

In this study, the CN3-peptide will be tested on its binding affinity to various types of fibrillar collagens and other ECM proteins. Since collagen types I and III are abundantly expressed in the fibrotic TME, this report will mainly focus on these types of fibrillar collagens. Furthermore, the peptide will be examined for its binding affinity *in vitro* and *ex vivo* using activated human pancreatic stellate cells (hPaSteCs), the main CAF-precursor cells in PDAC, and tissue sections of mice bearing PDAC, respectively. Thereafter, the CN3-peptide will be coupled to liposomes, consisting of HSPC lipids, DSPE-PEG lipids, DSPE-PEG-DBCO lipids and cholesterol, to actively target the TME [71]. Liposomes are known to have good biocompatibility, low toxicity, and ease of functionalization [71]. The payload flexibility and the fact that many liposome-based formulations are already approved by the Food and Drug Administration (FDA), make these type of carrier an interesting candidate [72, 73]. After optimizing and characterizing the CN3-coupled liposomes, its binding affinity will be tested on collagen-coated plates and an uptake study will be performed using collagen-coated plates and phagocytic cells. The eventual goal is to develop novel collagen-binding nanoparticles that could modify various players in the TME which is schematically depicted in figure 4.

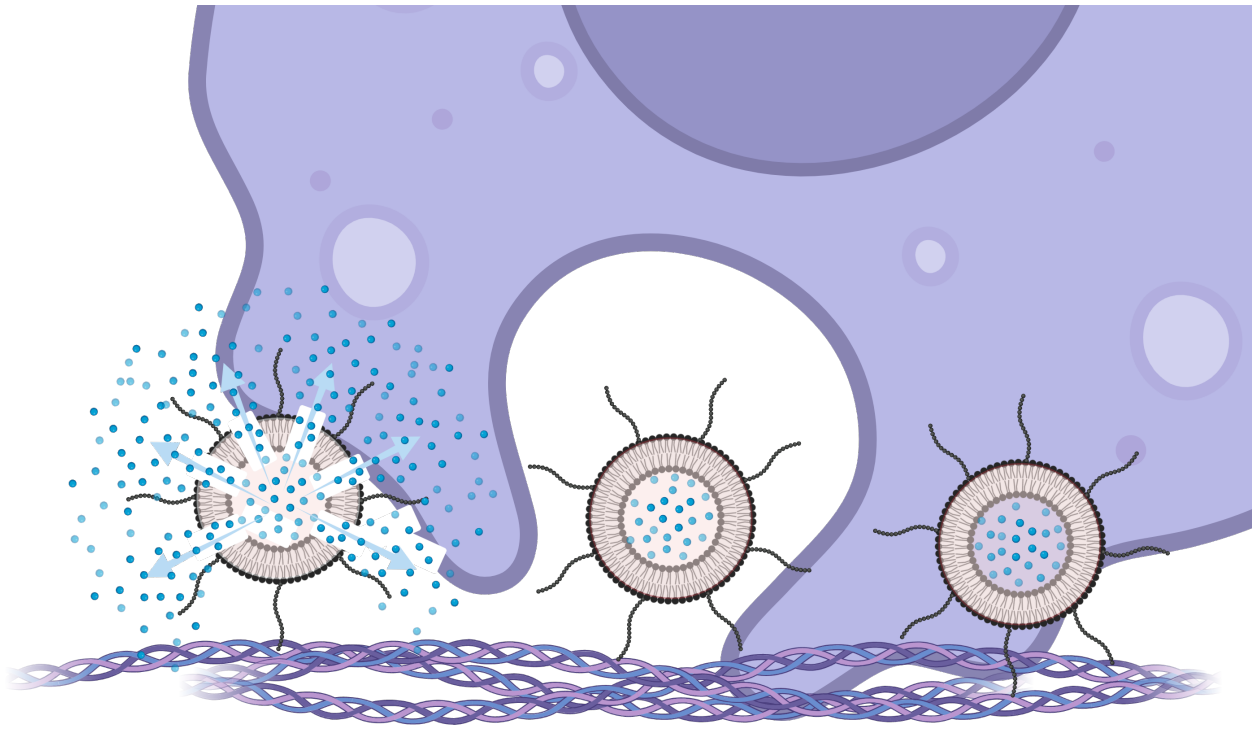

Figure 4: Schematic representation of the goal of the project. Collagen-bound drug-loaded liposomes can degrade and release its contents, or collagen-bound drug-loaded liposomes can be engulfed and alter behavior of the cells in the fibrotic TME.

2 Materials & Methods

2.1 Materials

Human collagen type III (C4407 and CC054) and human collagen type I (CC050) were purchased from Merck KGaA (Darmstadt, Germany). Human fibronectin was obtained from RD systems (RD Systems, Inc., Minneapolis, MN, Canada) and human collagen type II (Abcam, Cambridge, UK) was kindly provided by the DBE group at the University of Twente. Bovine collagen type I solution G1 was purchased from MATRIX BioScience GmbH (Mörlenbach, Germany). 3, 3′,5 ,5′-Tetramethylbenzidine Liquid Substrate, Supersensitive (T4444) and HRP-Streptavidin (RABHRP3) were purchased from Merck KGaA (Darmstadt, Germany). Hydro Soy Phosphatidylcholine (HSPC), Lipoid PE 18:0/18:0 PEG-2000 (DSPE-PEG(2000)), 1,2-distearoyl-sn-glycero-3-phosphoethanolamine-N-[dibenzocyclooctyl(poly ethylene glycol)-2000] (ammonium salt) (DSPE-PEG(2000)-DBCO) were purchased from Avanti Polar Lipids (Alabaster, AL, USA). Cholesterol was purchased from Merck KGaA (Darmstadt, Germany) and 1,1'-Dioctadecyl-3,3,3',3'-Tetramethylindocarbocyanine Perchlorate ('DiI'; DiIC18(3)) was obtained from Thermo Fisher Scientific Inc. (Waltham, MA, USA). Neutravidin and biotin was kindly provided by the DBE group at the University of Twente. Goat Anti-Type I Collagen-UNLB (1310-01) and Goat Anti-Type III Collagen-UNLB (1330-01) were obtained from SouthernBiotech (Birmingham, AL, USA). Streptavidin-Alexa Fluor™ 488 conjugate (16891) was purchased from AAT Bioquest® (Sunnyvale, CA, USA) and donkey anti-Goat IgG (H+L) Cross-Adsorbed Secondary Antibody Alexa Fluor 594 (A11058) was purchased from Thermo Fisher Scientific Inc. (Waltham, MA, USA). CN3, CN3-PEG(6)-biotin, and CN3-azide were obtained from China Peptide Co. Ltd. (Shanghai, China).

2.2 Cells

Human pancreatic stellate cells (hPaSteCs) were purchased from ScienCell™ (Carlsbad, CA, USA) and maintained in Stellate Cell Medium (SteCM) supplemented with 2% v/v FBS, 1% v/v SteCGS, and 1% v/v Penicillin-Streptomycin. KPC Cell Line (C57/BL6 genetic background) were purchased from Ximbio (London, UK) and maintained in Gibco™ DMEM/F-12 (Thermo Fisher Scientific Inc., Waltham, MA, USA) supplemented with 10% v/v FBS, 1% v/v L-glutamine, and 1% v/v Penicillin-Streptomycin.

2.3 Peptide identification and binding experiments

2.3.1 Peptide membrane array experiments

PepSPOTs™ cellulose membranes containing different sequences of potential collagen type III-binding peptides were obtained from JPT Peptide Technologies GmbH (Berlin, Germany). The membranes were soaked in methanol for 1 minute followed by a three-times rinse in TBS pH 8.0. The membranes were then incubated in a blocking solution consisting of 3% bovine serum albumin (BSA) in TBS with 0.05% Tween 20 (TBST) for 3 hours at room temperature. After washing once in TBST for 10 minutes, the membranes were incubated overnight with human collagen type III (Merck KGaA, Darmstadt, Germany) or bovine collagen type I (Collagen G1, MATRIX BioScience GmbH, Mörlenbach, Germany) at a concentration of 5 μg/ml in 3% BSA in TBST at 4°C. On the next day, membranes were washed thrice in TBST and further incubated with goat anti-collagen type III or type I antibodies (SouthernBiotech, Birmingham, AL, USA) in a 1:1000 dilution in 3% BSA in TBST for 3 hours at room temperature. After three-times wash in TBST, the membranes were incubated with rabbit anti-goat Immunoglobulins/HRP at a dilution of 1:2000 in 3% BSA in TBST for 1 hour at room temperature. Thereafter, the membranes were washed four times in TBST and chemiluminescence was developed using the SuperSignal™ West Pico PLUS Chemiluminescent substrate (Thermo Fisher Scientific Inc., Waltham, MA, USA) and measured using the FluorChem M system (ProteinSimple, San Jose,

CA, USA). Membranes were regenerated in Restore™ Western Blot Stripping Buffer (Thermo Fisher Scientific Inc., Waltham, MA, USA).

2.3.2 Binding affinity assay

The binding affinity of the CN3-peptide was examined using a modified enzyme-linked immunosorbent assay (ELISA). A ninety-six-well ELISA plate (Nunc™ MediSorp) was coated with human collagen type III (Merck KGaA, Darmstadt, Germany), type I bovine collagen solution (Collagen G1, MATRIX BioScience GmbH, Mörlenbach, Germany), human collagen type II (Abcam, Cambridge, UK), and human fibronectin (RD Systems, Inc., Minneapolis, MN, Canada) at 10 μg/ml and left at room temperature for 2 hours under continuous shaking at 225 RPM followed by incubation at 4°C overnight. All types of collagens were diluted in 0.01 N HCl and fibronectin was diluted in 1x PBS. On the next day, unbound collagen-solution was then discarded, and the wells were washed twice with 0.05% Tween 20 in PBS (PBST). After blocking the wells with 2% BSA in PBS for 1 hour at room temperature using a shaker at 225 RPM, the wells were washed twice with PBST and further incubated with increasing concentrations of CN3-PEG(6)-biotin with or without a 10-times molar excess of the non-biotinylated CN3-peptide in 1% BSA in PBS for 2 hours at room temperature using a shaker at 225 RPM. Then, the wells were washed three times with PBST, followed by an incubation with 1:4000 or 1:400 HRP-Streptavidin (Merck KGaA, Darmstadt, Germany) diluted in 2% BSA in PBS at room temperature for 1 hour using a shaker at 225 RPM. After thoroughly washing the wells, the bound CN3-PEG(6)-biotin was detected using 3, 3′,5 ,5′-Tetramethylbenzidine Liquid Substrate, Supersensitive (Merck KGaA, Darmstadt, Germany). After sufficient color development, the reaction was stopped using 2 N H_2SO_4 and the absorbance was measured at 450 nm with subtraction of the background-absorbance at 570 nm. The K_D-values were estimated by fitting the Hill-equation (equation 1), assuming one-site-specific binding, to the data using nonlinear curve fitting in Origin® 2019b (OriginLab Corporation, Northampton, MA, USA).

$$\theta = \frac{[L]^n}{K_D + [L]^n} \tag{1}$$

Where:
θ = fraction occupied receptor concentration to total receptor concentration
$[L]$ = total ligand concentration
K_D = dissociation constant
n = Hill coefficient

2.4 *In vitro* and *ex vivo* binding studies

2.4.1 *In vitro* modified immunofluorescence on hPaSteCs

hPaSteCs were seeded in a 24-well plate at cell density of 5,000 cells per cm^2 in complete SteCM. After 24 hours, the wells were washed once with DPBS and further incubated in serum-free SteCM. On the next day, the medium was changed by serum-free SteCM supplemented with 5 ng/ml TGF-β1 (RD Systems, Inc., Minneapolis, MN, Canada) to activate the quiescent hPaSteCs. After 48 hours incubation, the wells were washed once and fixed ice-cold acetone/methanol (1:1) for 30 minutes at -20°C. The acetone/methanol was then discarded, and the plate was dried, using a conventional hairdryer, for 30 minutes. A Dako or PAP pen (Agilent Technologies, Santa Clara, CA, USA) was used to mark a hydrophobic barrier around the edges of the sections to limit the amount of antibody-solution during incubation. When the hydrophobic barrier was dry, the cells were rehydrated in PBS for 5 minutes followed by blocking of unspecific sites using a 2% BSA solution in PBS for 1 hour at room temperature using a shaker at 150 RPM. The BSA solution was then discarded and goat anti-collagen types I and III antibodies (SouthernBiotech,

Birmingham, AL, USA), diluted in 1% BSA in PBS, were added to the wells. After incubation with the antibodies for 1 hour at room temperature using a shaker at 150 RPM, the wells were washed thrice with PBS and incubated with CN3-PEG(6)-Biotin at a concentration of 5 μM for 1 hour at room temperature using a shaker at 150 RPM. After washing thrice, 5 μg/ml streptavidin-Alexa Fluor™ 488 (Thermo Fisher Scientific Inc., Waltham, MA, USA) and 1:100 dilution of donkey anti-goat Alexa Fluor™ 594 (Thermo Fisher Scientific Inc., Waltham, MA, USA) in 1% BSA were added to the wells for 1 hour at room temperature using a shaker at 150 RPM. The wells were washed for five consecutive times and mounted in Fluoroshield™ with DAPI (Merck KGaA, Darmstadt, Germany). A coverslip was added to each well and the wells were analyzed using the EVOS cell imaging system (Thermo Fisher Scientific Inc., Waltham, MA, USA). Images were further processed and quantified in ImageJ. Colocalization was measured using the JACoP-plugin by Bolte *et al.* [74].

2.4.2 *In vitro* modified immunofluorescence on deposited collagen by hPaSteCs

hPaSteCs were seeded in a tissue-culture treated 24-well plate at cell density of 5,000 cells per cm^2 in complete SteCM. After 24 hours, the wells were washed once with DPBS and further incubated in serum-free SteCM. On the next day, the medium was changed by serum-free SteCM supplemented with or without 5 ng/ml TGF-β1 (RD Systems, Inc., Minneapolis, MN, Canada) and 100 μg/ml Dextran Sulfate (DxS) sodium salt >500 kDa (Merck KGaA, Darmstadt, Germany). After 48 hours incubation, the wells were washed once and fixed in 4% formaldehyde for 15 minutes at room temperature. Then, the wells were washed thrice and kept in PBS at 4°C until used. When the staining proceeded, the PBS was removed and a Dako or PAP pen (Agilent Technologies, Santa Clara, CA, USA) was used to mark a hydrophobic barrier around the edges of the sections to limit the amount of antibody-solution during incubation. When the hydrophobic barrier was dry, the cells were incubated with a 2% BSA solution in PBS for 1 hour at room temperature using a shaker at 150 RPM. The BSA solution was then discarded and goat anti-collagen types I and III antibodies (SouthernBiotech, Birmingham, AL, USA), diluted in 1% BSA in PBS, were added to the wells. After incubation with the antibodies for 1 hour at room temperature using a shaker at 150 RPM, the wells were washed thrice with PBS and incubated with CN3-PEG(6)-Biotin at a concentration of 5 μM for 1 hour at room temperature using a shaker at 150 RPM. After washing thrice, 5 μg/ml streptavidin-Alexa Fluor™ 488 (Thermo Fisher Scientific Inc., Waltham, MA, USA) and 1:100 dilution of donkey anti-goat Alexa Fluor™ 594 (Thermo Fisher Scientific Inc., Waltham, MA, USA) in 1% BSA were added to the wells for 1 hour at room temperature using a shaker at 150 RPM. The wells were washed for five consecutive times and mounted in Fluoroshield™ with DAPI (Merck KGaA, Darmstadt, Germany). A coverslip was added to each well and the wells were analyzed using the EVOS cell imaging system (Thermo Fisher Scientific Inc., Waltham, MA, USA). Images were further processed and quantified in ImageJ. Colocalization was measured using the JACoP-plugin by Bolte *et al.* [74].

2.4.3 *Ex vivo* modified immunofluorescence in pancreatic tumor cryosections

Cryosections of mice bearing PDAC were obtained from animal experiments using the KPC mouse model [75]. Frozen tissue sections on microscopy slides were dried using a hairdryer and were then fixed in pre-cooled acetone (-20°C) for 10 minutes at room temperature. The slides were then air dried and a Dako or PAP pen (Agilent Technologies, Santa Clara, CA, USA) was used to mark a hydrophobic barrier around the edges of the sections to limit the amount of antibody-solution during incubation. Once the hydrophobic barrier was dry, the sections were hydrated in using 1x PBS for 5 minutes. Then, a 2% BSA solution with 200 μg/ml neutravidin (Merck KGaA, Darmstadt, Germany) in PBS was used to block unspecific sites and endogenous biotins, respectively, for 1 hour at room temperature. The sections were washed thrice using 1x PBS and the remaining binding sites of neutravidin were blocked by incubating the sections with 2% BSA solution supplied with 50 μg/ml biotin (Merck KGaA, Darmstadt, Germany) for 1 hour at room temperature. After washing the sections thrice, the sections were incubated overnight at 4°C with or without 2.5

μM CN3-PEG(6)-biotin and goat anti-collagen type I and/or III antibodies (SouthernBiotech, Birmingham, AL, USA) diluted in 1% BSA in PBS. After washing thrice, 5 μg/ml streptavidin-Alexa Fluor™ 488 (Thermo Fisher Scientific Inc., Waltham, MA, USA) and 1:100 dilution of donkey anti-goat Alexa Fluor™ 594 (Thermo Fisher Scientific Inc., Waltham, MA, USA) in 1% BSA were added to the sections for 1 hour at room temperature. The sections were washed for four consecutive times and mounted in Fluoroshield™ with DAPI (Merck KGaA, Darmstadt, Germany). A coverslip was added, and the sections were analyzed using the Zeiss LSM 880 confocal microscope (Carl Zeiss AG, Oberkochen, Germany). Images were further processed in ImageJ.

2.5 Preparation and characterization of (peptide-coupled) PEGylated liposomes

2.5.1 Preparation of (peptide-coupled) PEGylated liposomes

Liposomes were produced according to the ethanol-injection method followed by extrusion to downsize the liposomes [76]. In brief, HSPC, cholesterol, Lipoid PE 18:0/18:0-PEG 2000, and DSPE-PEG(2000)-DBCO were mixed in a molar ratio of 6.5:3:0.4:0.1 which was determined experimentally (table A1) and partly derived from literature [77, 78]. Liposomes without DSPE-PEG(2000)-DBCO contained 5 mol% Lipoid PE 18:0/18:0-PEG 2000 and when fluorescent labeling of liposomes was desired, 1 mol% of lipid soluble DiI was added to the lipid mixture. Then, all lipids and dyes were dissolved in absolute ethanol at 10% v/v of the final volume using a block-heater at 70°C. At the same time, 1x PBS (90% v/v of final volume) was pre-warmed to 70°C. When the lipid mixture was dissolved completely and the PBS was pre-warmed, the lipid mixture was injected into the pre-warmed PBS while vortexing vigorously. After obtaining crude liposomes when injecting the lipid mixture in the PBS, the liposomes were downsized using the LiposoFast LF-50 extruder (Avestin Inc., Ottawa, ON, Canada). The liposomes without DBCO were extruded through Whatman® Nucleopore™ Track-Etched Membranes (Merck KGaA, Darmstadt, Germany) for 10 times by starting with a combination of 0.4-0.4 μm, followed by 0.2-0.2 μm, and finally 0.1-0.1 μm. DBCO-containing liposomes were extruded 19 times starting with a membrane combination of 0.4-0.4 μm, followed by 0.2-0.2 μm, 0.1-0.1 μm, and 0.08-0.08 μm to obtain the desired hydrodynamic diameter of around 100 nm. Coupling of the azide-modified peptides to the DBCO-group on the liposomes was accomplished using copper-free click chemistry using strain-promoted azide–alkyne cycloaddition reactions (SPAAC) [79]. In short, a four-times molar excess of azide-modified CN3-peptide to DSPE-PEG(2000)-DBCO was added to the extruded liposomes containing DBCO. The mixture was then diluted 1 to 1 in 1x PBS and then left on a roller for 2 hours at RT, followed by incubation on a roller overnight at 4°C. After 24 hours, 20 μL of the mixture was diluted 5 times and then ultracentrifuged for 2 hours at 100,000 $\times$ g at 4°C using the Sorvall™ WX-80 supplied with a Fiberlite™ F50L-24 x 1.5 rotor (Thermo Fisher Scientific Inc., Waltham, MA, USA). After centrifugation, the supernatant was collected for coupling-efficiency measurements. The rest of the volume, containing the liposomes and the azide-conjugated peptides, was dialyzed overnight at 4°C against 1x PBS using a Slide-A-Lyzer™ MINI Dialysis Device 20K MWCO (Thermo Fisher Scientific Inc., Waltham, MA, USA) to remove unbound peptide.

2.5.2 Size, polydispersity index, and zeta potential measurements

The hydrodynamic diameter and polydispersity index (PDI) of the liposomes were measured by Dynamic Light Scattering (DLS) using the ZetaSizer Nano ZS equipped with a 633 nm HeNe laser (Malvern Panalytical Ltd., Malvern, UK). The original liposome suspensions were diluted 1:50 or 1:100 in 1x PBS and equilibrated for at least 5 minutes before measuring at 25°C. The zeta potential (ζ-potential) was determined by Electrophoretic Light Scattering (ELS) using the ZetaSizer Nano ZS equipped with a 633 nm HeNe laser. The original liposome suspensions were diluted 1:50 or 1:100 in 10 mM KCl and placed in a folded capillary zeta cell (Malvern Panalytical Ltd., Malvern, UK). The dilutions were equilibrated for at least 5 minutes before measuring at 25°C.

2.5.3 Peptide coupling-efficiency

The absorbance at 205 nm of known concentrations of CN3-azide in 1x PBS was measured before and after all measurements to establish a calibration curve using the Shimadzu UV-2401 PC (Shimadzu corporation, Kyoto, Japan). Then, the collected supernatant was diluted 1:10 in 1x PBS and measured for absorbance at 205 nm. The coupling-efficiency (CE%) was calculated using equation 2.

$$CE\% = (mf \times (1 - (\frac{C_m \times df}{C_i}) \times 100\% \quad (2)$$

Where:
CE% = estimated coupling-efficiency (%)
mf = molar excess factor of azide-conjugated peptide to DBCO
C_m = measured concentration (μM)
C_i = initial concentration (μM)
df = total dilution factor of the collected supernatant

2.5.4 Liposomal stability

The stability of the DBCO-liposomes and the peptide-conjugated liposomes at storage temperature (i.e., 4°C) was evaluated by DLS at fixed timepoints. The hydrodynamic diameter and the PDI were measured according to section 3.5.2.

2.6 Liposome binding studies

2.6.1 Binding affinity assay

A ninety-six-well ELISA plate (Nunc™ MediSorp) was coated with human collagen type III (Merck KGaA, Darmstadt, Germany), type I bovine collagen solution (Collagen G1, MATRIX BioScience GmbH, Mörlenbach, Germany) at 10 μg/ml in 0.01 N HCl and left at room temperature for 2 hours followed by incubation at 4°C overnight. On the next day, unbound collagen-solution was then discarded, and the wells were washed twice with 1x PBS. After blocking the wells with 2% BSA in PBS for 1.5 hours at room temperature using a shaker at 225 RPM, 100 μl of approximately 200 μM DiI-containing PEGylated liposomes and CN3-coupled liposomes in 1% BSA in PBS with or without a 50-times molar excess of CN3-peptide were added to the wells and incubated for 2 hours at room temperature using a shaker at 225 RPM. Before adding the liposomes to the wells, the fluorescent intensity was set equal for both formulations. Then, the wells were washed trice with PBST and 100 μl DMSO was added to each well. After 5 minutes of incubation at room temperature using a shaker at 225 RPM, the content of each well was transferred to a black clear F-bottom ninety-six-well plate (Greiner Bio-One, Kremsmünster, Austria) for fluorescent measurements. The fluorescent intensity was measured using a TECAN Infinite® 200 Pro (Tecan Group Ltd., Switzerland). The excitation wavelength was 530 nm, and the emission wavelength was 567 nm.

2.6.2 *In vitro* binding studies

Type I bovine collagen solution (Collagen G1, MATRIX BioScience GmbH, Mörlenbach, Germany) was diluted in sterile 0.01 N HCl to a recommended concentration of 38 μg/ml to obtain a collagen amount of 10 μg/cm^2. Tissue-culture treated 24-well plates were coated with the diluted type I collagen and left at room temperature for 2 hours followed by incubation at 4°C overnight. The unbound collagen-solution was then aspirated, and the wells were washed twice with DPBS. After blocking the wells with sterile 2% BSA in PBS for 1 hour at room temperature using a shaker

at 150 RPM, the wells were washed once with DPBS, and 300 μl of approximately 1500 μM DiI-containing PEGylated liposomes and CN3-coupled liposomes in sterile PBS were added to the wells. The liposomes were incubated at room temperature for 2 hours using a shaker at 150 RPM. The wells were then washed twice with sterile PBST and once with DPBS. Then, non-activated hPSteCs were seeded in the wells at a cell density of 2,500 cells per cm^2 in complete SteCM and incubated at 37°C for 20 hours. The wells were washed twice with DPBS and 300 μl of trypsin was added to each well to detach the cells. Trypsin was then neutralized using 1000 μl of complete SteCM and the content of each well was collected in a FALCON® round-bottom polystyrene test tube (Corning Inc., NY, USA). More precise, the content of three wells of the same condition were collected in one tube which had a cell count of >10,000 cells. The tubes were centrifuged at 300 $\times$ g for 5 minutes and the supernatant of each tube was then aspirated. After resuspending the cells in 200 μl DPBS, the sample was ready for flow cytometry analysis using the MACSQuant® VYB Flow Cytometer (Miltenyi Biotec, Bergisch Gladbach, Germany). In brief, forward (FSC) and side scatter (SSC) were measured, and cells were gated to separate the live cells from the cell debris in Flowing Software version 2.5.1 (Turku Bioscience, Turku, Finland). Simultaneously, the fluorescence in channel PE-A (Y1: 586/15 nm) was used to measure the mean fluorescent intensity per sample.

2.7 Statistical analysis

The data is presented as mean ± standard deviation (SD). Statistical analyses were performed using Origin® version 2019b (OriginLab Corporation, Northampton, MA, USA). To assess differences between groups, one-way analyses of variances (ANOVA) were performed, and the data was considered statistically significant at $p<0.05$ ($*$), $p<0.01$ ($**$), and $p<0.001$ ($***$).

3 Results

3.1 Binding of CN3-peptide to collagen types I and III

Earlier in the group, the CN3-peptide was designed using interaction studies between mannose receptor and collagen. In this experiment, the binding of the CN3-peptide was further confirmed using a PepSPOTs™ cellulose membrane containing different sequences of potential collagen type III-binding peptides. In short, the membranes were incubated with either collagen type I or collagen type III. Then, the membranes were washed and incubated with antibodies against either collagen type I or collagen type III. The last steps included the addition of HRP-conjugated secondary antibodies and development of chemiluminescence.

As depicted in figure 5A, signal is observed for the CN3-peptide for both collagens type I and type III while peptide X, another candidate for binding to collagen type III, did not show any signal. As peptide X did not show any signal, the signal of the CN3-peptide was compared to that of peptide X. From the bar diagram in figure 5B, the CN3-peptide showed a 3.5-fold increase in signal as compared to peptide X for collagen type I, while a 6.5-fold increase in signal was observed in collagen type III. Results suggests that the CN3-peptide binds to both collagen type I and collagen type III.

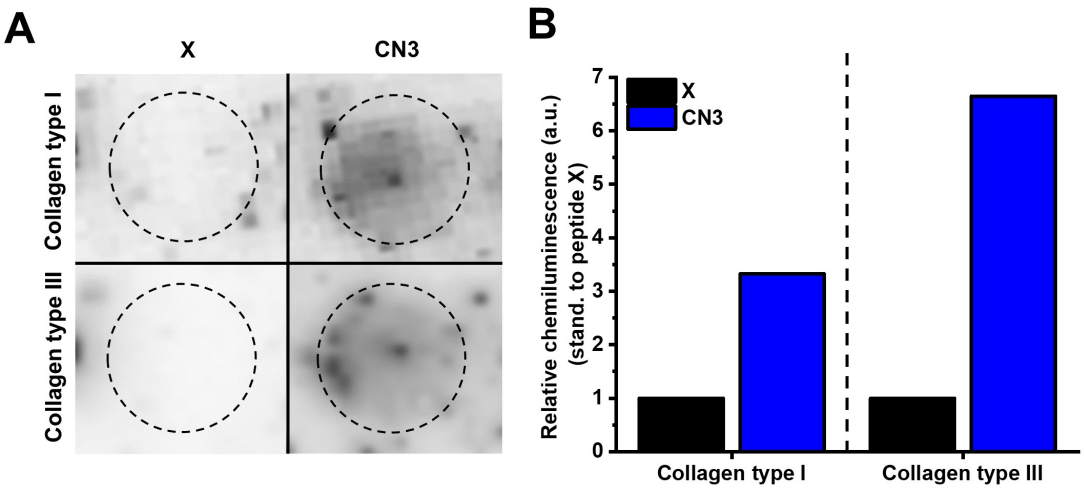

Figure 5: CN3-peptide binding to collagen types I and III. A) Chemiluminescence observed in peptide X and the CN3-peptide for collagen type I and collagen type III (n=1). B) Relative chemiluminescence standardized to peptide X (n=1).

3.2 Binding of CN3-peptide to plates coated with collagen and fibronectin

To evaluate the binding affinity of the CN3-peptide, a direct modified ELISA was performed. In brief, various types of collagens were coated on ELISA plates and incubated with the biotinylated CN3-peptide (CN3-biotin). Then, HRP-conjugated streptavidin was added, and color was developed using TMB substrate. Absorbance was measured and the K_D-values were estimated by fitting the Hill equation assuming one-site-specific binding.

For both collagen type I and collagen type III, the absorbance increased with concentration CN3-biotin, as depicted in figure 6A. The absorbance values for collagen type III appeared to be higher as compared to collagen type I, suggesting a better binding of the CN3-biotin to collagen type III. The estimated K_D-values were 222 ± 37 nM and 195 ± 10 nM for bovine collagen type I and human collagen type III, respectively. In an earlier experiment, the K_D-value was determined at 113 ± 58 nM, which indicates even better binding to collagen type III (figure A1A). In earlier conducted experiments in which collagen was coated at a concentration of 2 μg/ml and CN3-biotin was not mixed with 2% BSA before incubation, human collagen type I showed K_D-value of 261 ± 35 nM (figure A1B). All experiments suggest that CN3-biotin binds to both types of collagens but preferably to collagen type III which consistent with the observations from figure 5A and 5B.

Exploring more binding characteristics of CN3-biotin, its affinity to few other ECM-proteins was tested as well (figure 6B). As the absorbance values for collagen type II and fibronectin were low, hardly any binding to fibronectin and collagen type II was observed. This indicates that the peptide does not show unspecific binding to other ECM-proteins. Further demonstrating specific binding to collagen type III, an experiment was performed in which CN3-biotin was blocked with a 10- and 50-times molar excess of CN3-peptide. From figure 6C, signal of CN3-biotin was significantly reduced. Points at which the s-shaped curve develops at the fastest rate showed statistically significant differences between CN3-biotin, 10-times molar excess CN3-peptide, and 50-times molar excess CN3-peptide ($p<0.001$). This indicates specificity of the CN3-peptide as it can be blocked on collagen type III-coated plates.

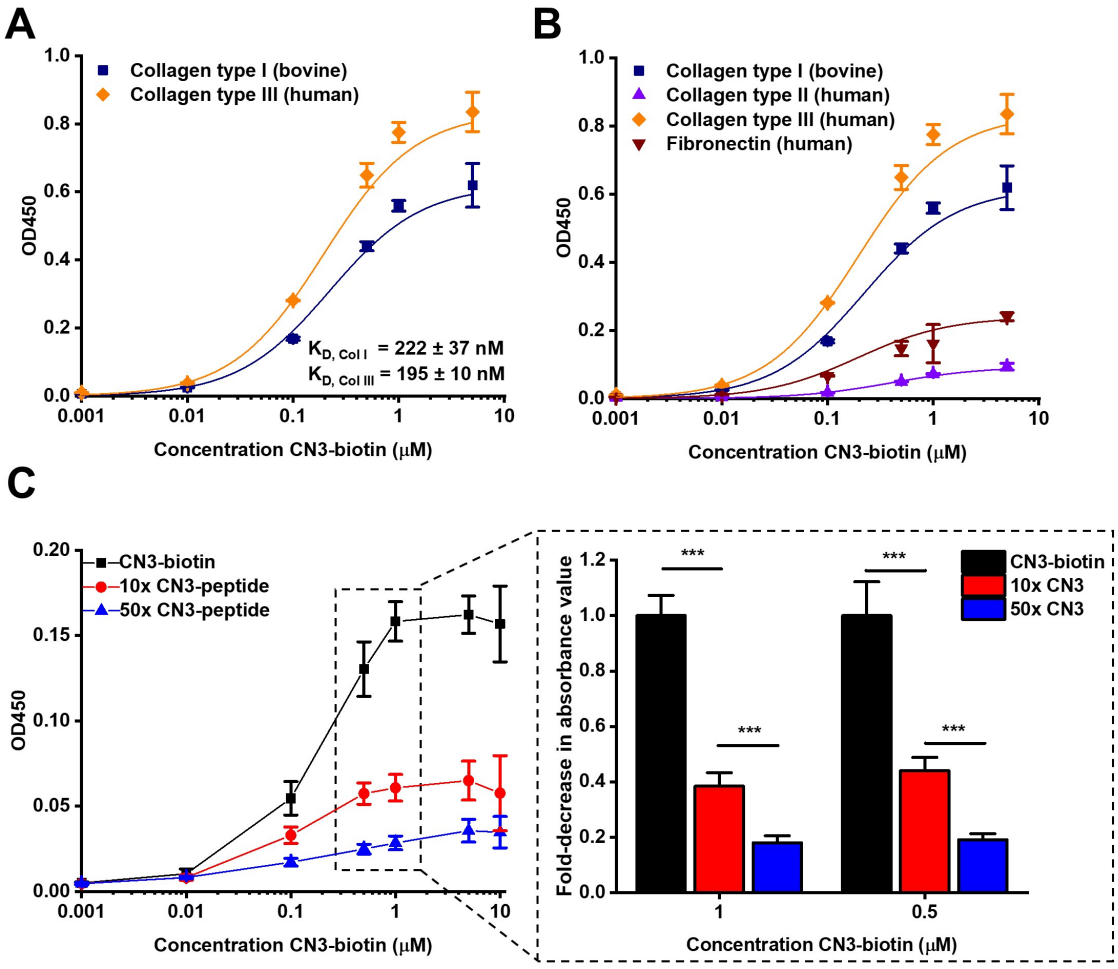

Figure 6: CN3-biotin binding experiments using ELISAs. A) Comparison between collagen type I and III in terms of absorbance and their estimated binding affinities (n=3). B) Comparison between collagen types I, II, III, and fibronectin (n=3). C) Measurements of absorbance on collagen type III using CN3-biotin and a 10- and 50-times molar excess of unconjugated CN3-peptide (n=6, 3 experimental replicates). Statistical analyses were done using analysis of variance (ANOVA). $***p<0.001$.

3.3 *In vitro* binding of the CN3-peptide to collagen-producing cells

Immunofluorescence on collagen-producing cells was conducted to visualize the binding of the CN3-peptide *in vitro*. In brief, hPaSteCs were seeded followed by starvation after 24 hours. Then, the cells were incubated with 5 ng/ml TGF-β1 in serum-free medium for 48 hours. Afterwards, the cells were fixed and stained for collagen type I and collagen type III. Simultaneously, the sections were incubated with the biotinylated CN3-peptide which was visualized using streptavidin-Alexa Fluor™ 488.

As depicted in figure 7, a higher production of collagen type I (figure 7A) as compared to collagen type III (figure 7B) by activated hPaSteCs was detected. Furthermore, most collagen was found intracellularly suggesting that simple *in vitro* cultures are not sufficient to mimic collagen production *in vivo*.

CN3-biotin appeared all over the cells with certain brighter areas, as indicated by the white arrows in figure 7A. Merging collagen type I with CN3-biotin showed clear colocalization while this was hard to detect by merging collagen type III with CN3-biotin, since collagen type III was expressed in low amounts. However, quantification of both collagens with CN3-biotin showed clear overlap in signal intensity plots (figures 8A and 8B). Calculating the Pearson correlation coefficient r, a measure for correlation between two variables, revealed a correlation higher than r=0.76 for both types of collagens (figure 8C). Moreover, correlation between collagen type III and CN3-biotin was significantly higher as compared to correlation between collagen type I and CN3-biotin (p<0.05), again suggesting that the peptide preferably binds to collagen type III. Interestingly, staining KPC cells as a negative control did not show any collagen production while lower concentrations CN3-biotin (i.e., 2 μM and 0.5 μM) did show similar staining patterns as observed in figure 7 (figure A2). These results suggest that CN3-biotin undergoes more interactions with the cells.

Quantification of the intensity of the CN3-biotin showed that blocking CN3-biotin with a 10-times molar excess of CN3-peptide revealed a statistically significant difference as compared to the wells without blocking (p<0.001, figure 8D). These results suggest that blocking with the CN3-peptide reduces signal intensity and binding of the CN3-biotin could be blocked *in vitro*.

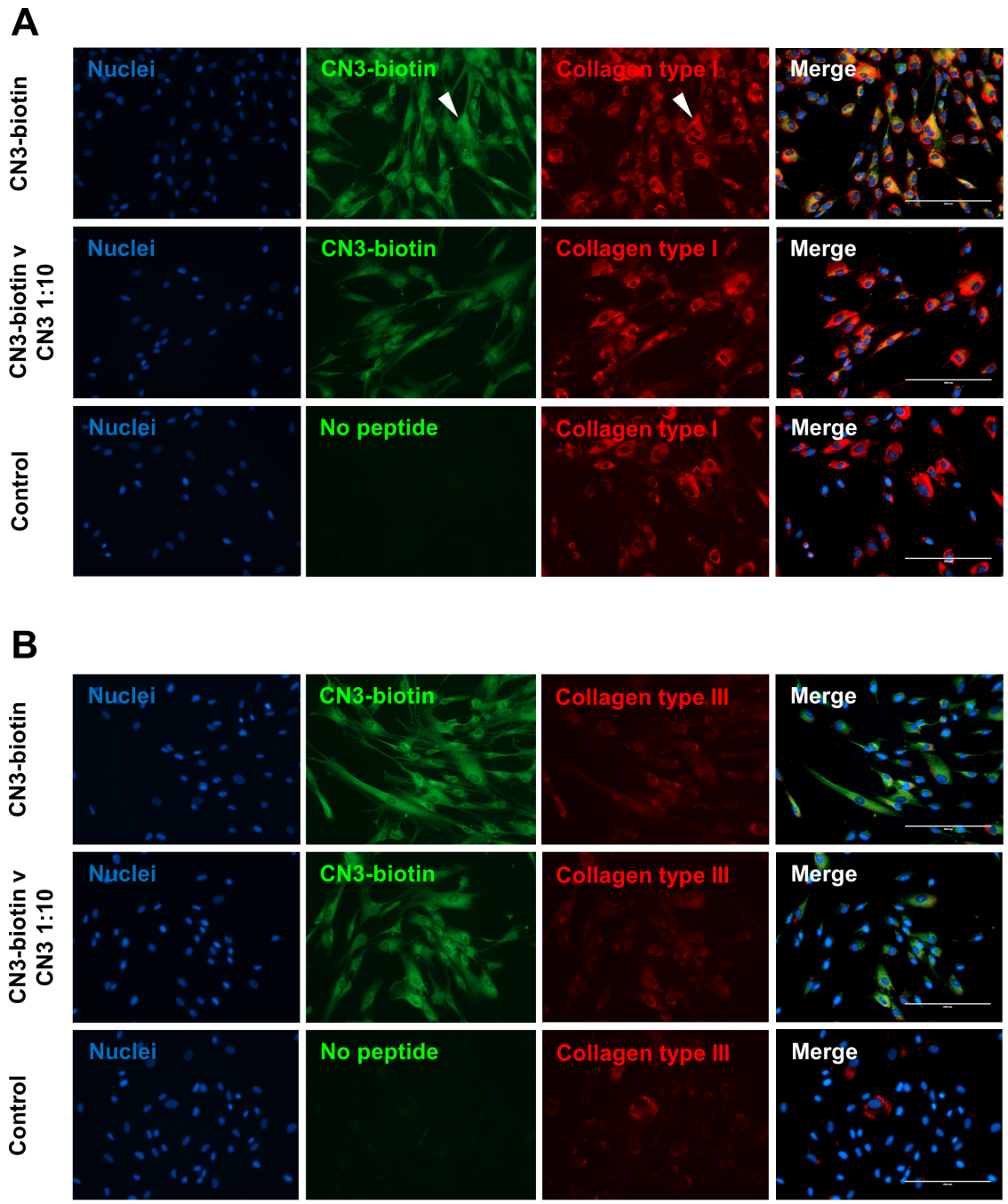

Figure 7: Immunofluorescence of activated hPaSteCs. A) Staining of TGF-β1 activated hPaSteCs with 4′,6-diamidino-2-phenylindole (DAPI, blue), CN3-biotin (green), and goat anti-collagen type I (red). CN3-biotin was stained with and without a 10-times molar excess of non-conjugated CN3-peptide. B) Staining of hPaSteCs with 4′,6-diamidino-2-phenylindole (DAPI, blue), CN3-biotin (green), and goat anti-collagen type III (red). CN3-biotin was stained with and without a 10-times molar excess of non-conjugated CN3-peptide. Representative images (n=3), scale bar = 200 μm.

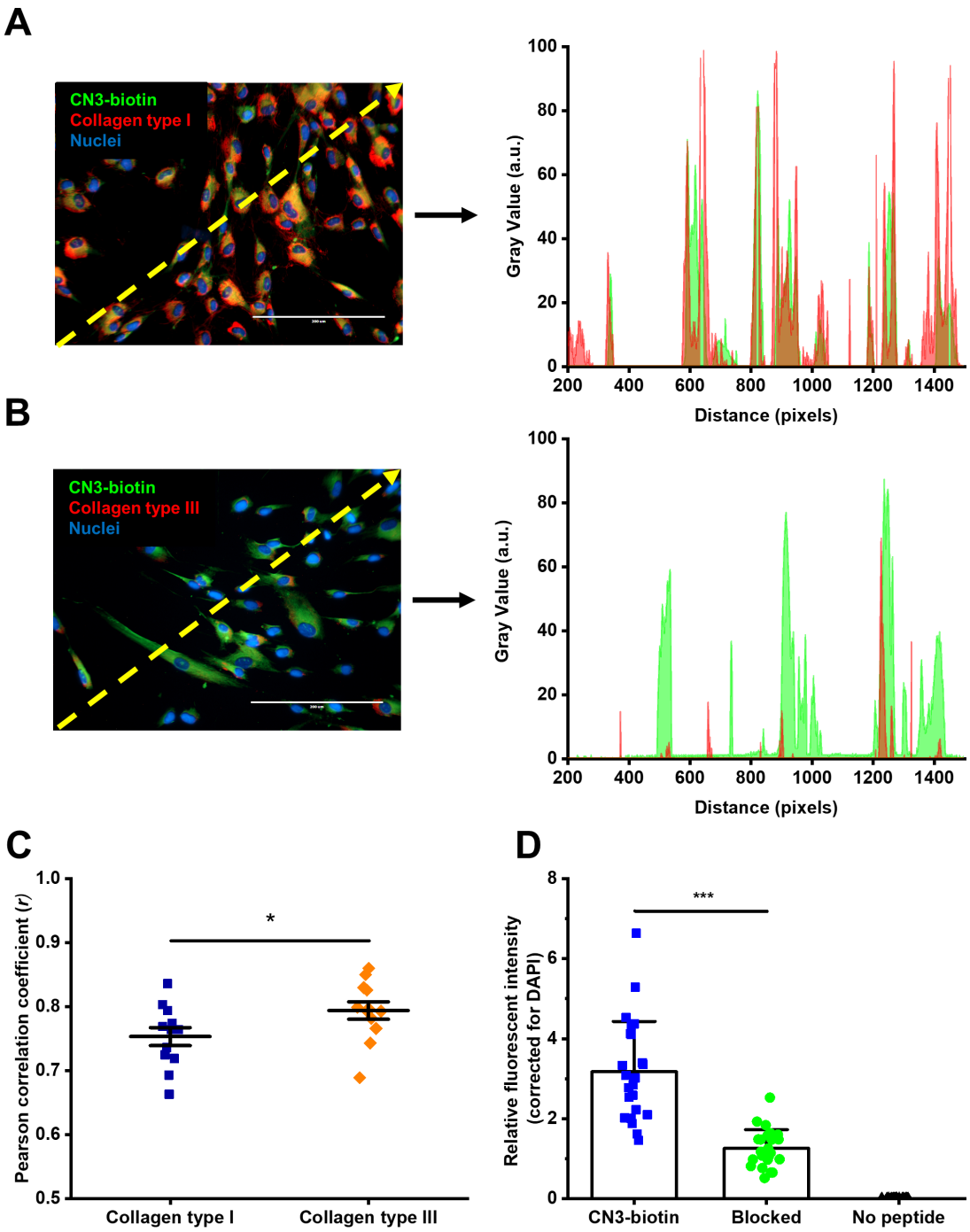

Figure 8: Quantification of the staining depicted in figure 7. A) Intensity plot showing the gray value per pixel for CN3-biotin (green) and collagen type I (red). B) Intensity plot showing the gray value per pixel for CN3-biotin (green) and collagen type III (red). C) Quantification of colocalization of CN3-biotin and both collagen types I and III using the Pearson correlation coefficient r (n=3, 4 measurements per well). D) Quantification of the fluorescent intensity for CN3-biotin, CN3-biotin with a 10-times molar excess of unconjugated CN3-peptide (blocked), and negative control (no peptide) (n=6, 4 images per well). Statistical analyses were done using analysis of variance (ANOVA). $*p<0.05$; $***p<0.001$.

3.4 *In vitro* binding of the CN3-peptide to cell-secreted collagen

Since the collagen and the CN3-peptide in figure 7 could only be found intracellularly, it was still unknown whether the CN3-peptide could bind to deposited, mature collagen. Therefore, methods for facilitating collagen deposition *in vitro* were utilized. Briefly, hPaSteCs were seeded and starved for 24 hours. Then, hPaSteCs were treated with 5 ng/ml TGF-β1 and 100 μg/ml macromolecular Dextran Sulfate, and further incubated for 48 hours. The cells were fixed and stained for collagen type I and collagen type III. Simultaneously, the sections were incubated with the biotinylated CN3-peptide which was visualized using streptavidin-Alexa Fluor™ 488.

As displayed in figure 9, an increased collagen deposition in hPaSteCs was observed, and this was verified by quantifying the collagen intensity (figure A3). In figure 9A, fragments of collagen could be observed in the samples with treatment. These collagen fragments were situated around and below the cells, as indicated by the grey arrows. However, in samples stained for collagen type III, the appearance of collagen fragments was not observed (figure 9B). Differences in collagen type I deposition between samples with and without treatment showed statistic significancy ($p<0.001$) while collagen type III did not, indicating that Dextran Sulfate has a function in the deposition of collagen type I. In general, collagen type I appeared more abundantly expressed as compared to collagen type III ($p<0.01$, figure A3).

In figure 9, CN3-biotin showed signal all over the cells, which was also observed in figure 7 and, as this signal was again detected in the samples without treatment, it gave further evidence that the CN3-biotin probably interacts with moieties in or on the cells. Merging the green and red channel showed overlap, but certain collagen fragments (grey arrows) did not seem to colocalize with the CN3-biotin (figure 9). As pointed out by the blue arrows, the pattern of the CN3-biotin appeared to be present in the red channel in the sample without treatment, while collagen type I was not present in that group as indicated by the sample without treatment and without peptide. The latter was also observed, and even more clear, in the samples with treatment stained for collagen type III, as pointed out by the green arrows (figure 9B). These results might suggest that the intensity of the green channel leaks into the red channel.

Colocalization was visualized using intensity plots and revealed certain overlap between the green and the red channel for both types of collagens (figure 10A and 10B). Interestingly, in places where collagen type I clearly showed signal, CN3-biotin was absent. Furthermore, the intensity plot for collagen type III showed almost perfect overlap between collagen type III and CN3-biotin which was verified by calculating the Pearson correlation coefficient r (figure 10C). The CN3-biotin showed significant higher colocalization with collagen type III as compared to collagen type I ($p<0.001$). However, as observed in figure 9B and figure A3, hardly any collagen type III was present, suggesting that the leaking of green channel into the red channel contributed to the observed Pearson correlation coefficient r. Interestingly, samples treated with both TGF-β1 and Dextran Sulfate which were stained with CN3-biotin revealed an increase in signal intensity as compared to the group without TGF-β1 and Dextran Sulfate ($p<0.001$, figure 10D).

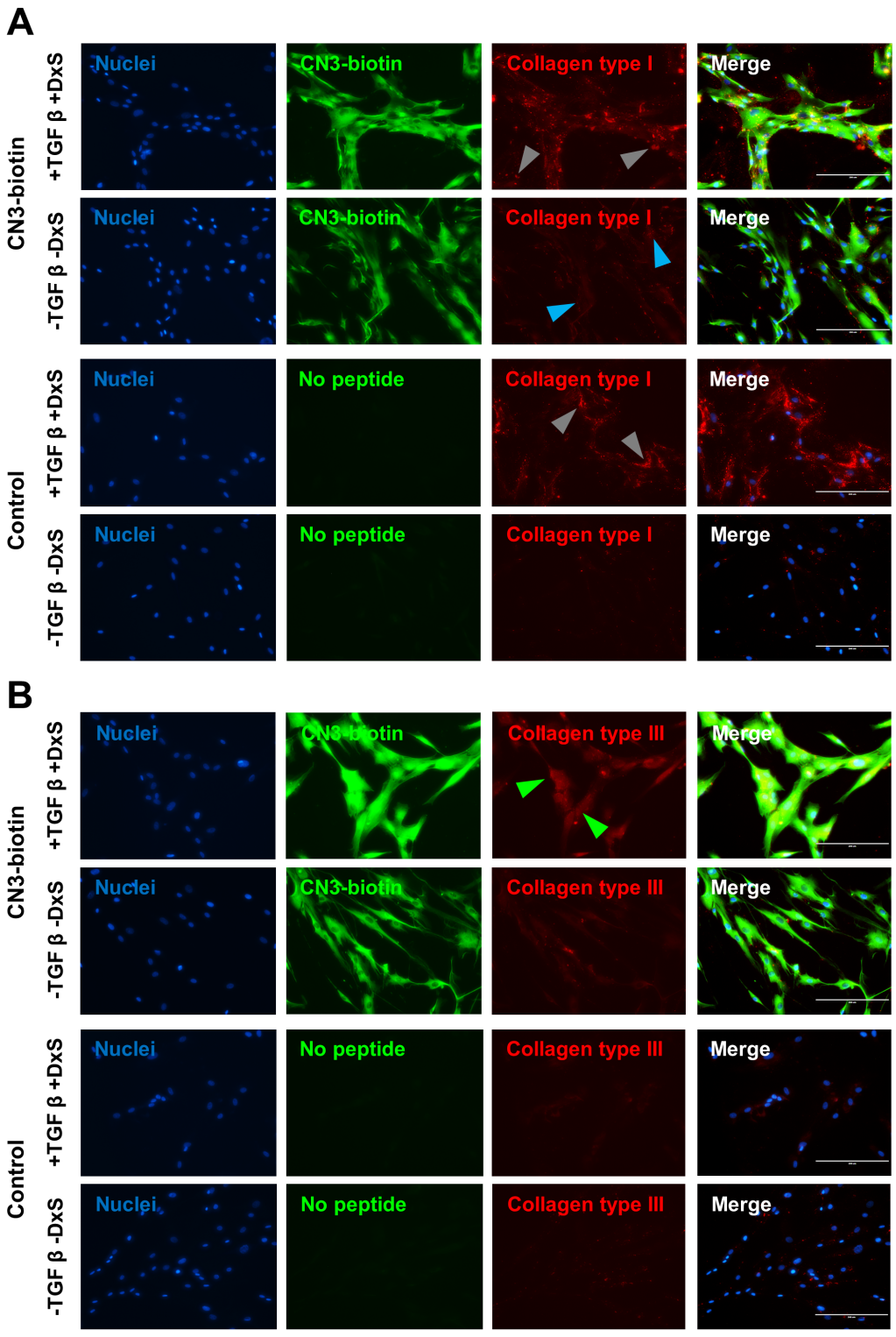

Figure 9: Immunofluorescence of activated and non-activated hPaSteCs (+TGF-β1, -TGF-β1) with or without Dextran Sulfate >500 kDa (+DxS, -DxS). A) Staining of deposited collagen by hPaSteCs with 4′,6-diamidino-2-phenylindole (DAPI, blue), CN3-biotin (green), and goat anti-collagen type I (red). B) Staining of collagen deposited by hPaSteCs with 4′,6-diamidino-2-phenylindole (DAPI, blue), CN3-biotin (green), and goat anti-collagen type III (red). Representative images (n=3), scale bar = 200 μm.

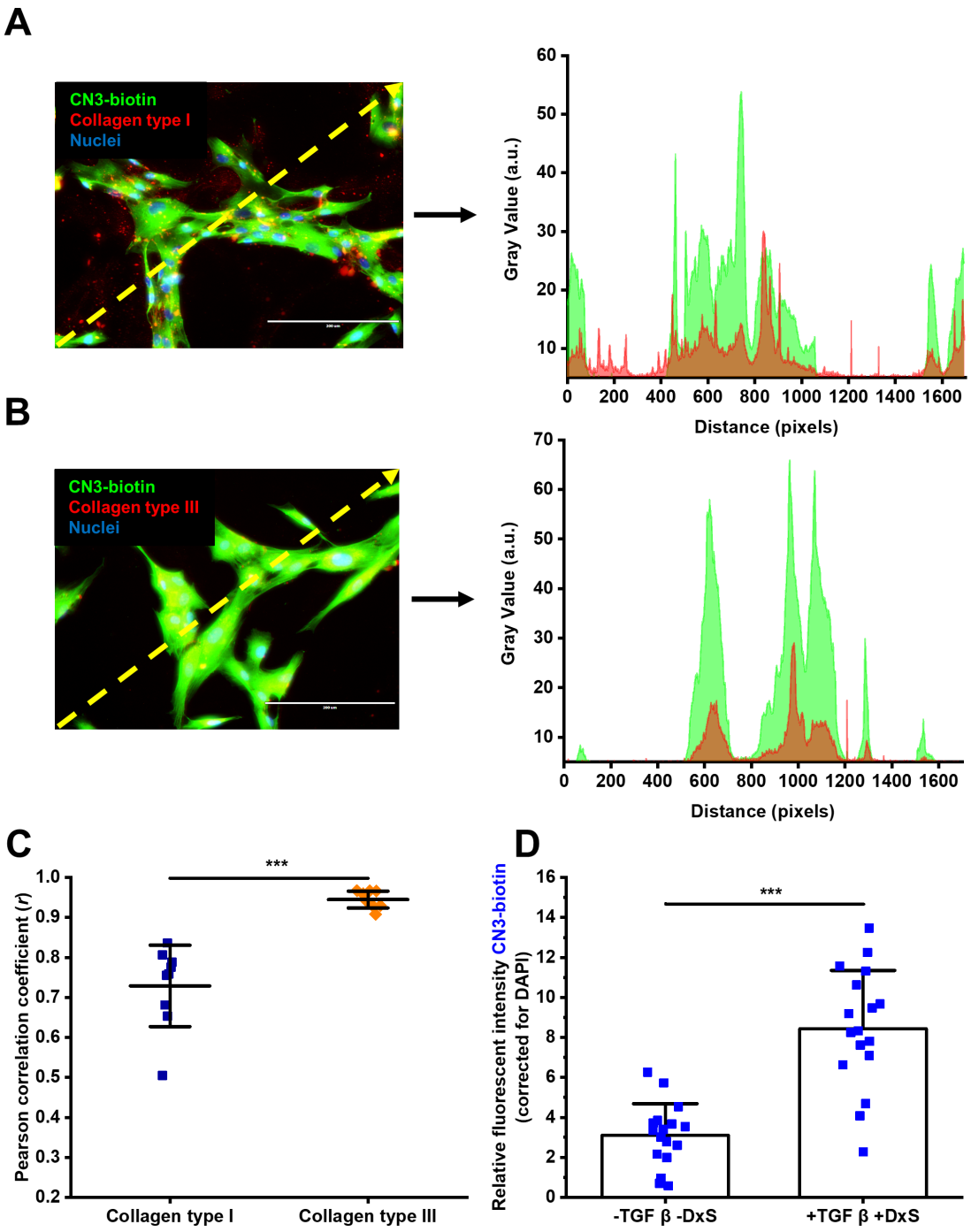

Figure 10: Quantification of the staining depicted in figure 9. A) Intensity plot showing the gray value per pixel for CN3-biotin (green) and collagen type I (red). B) Intensity plot showing the gray value per pixel for CN3-biotin (green) and collagen type III (red). C) Quantification of colocalization of CN3-biotin and both collagen types I and III using the Pearson correlation coefficient r (n=3, 3 images per well). D) Quantification of the fluorescent intensity for CN3-biotin in hPaSteCs when supplemented with TGF-β1 and DxS, and without both TGF-β1 and DxS (n=6, 3 images per well). Statistical analyses were done using analysis of variance (ANOVA). $***p<0.001$.

3.5 *Ex vivo* binding of the CN3-peptide in pancreatic tumor cryosections

Having difficulties to develop sufficient amounts of collagen type III *in vitro*, tissue sections from mice bearing PDAC were used in an ultimate attempt to visualize whether the CN3-peptide could bind to mature native collagen type I and III. In short, cryosections were fixed and stained for collagen type I and collagen type III. Simultaneously, the sections were incubated with the biotinylated CN3-peptide which was visualized using streptavidin-Alexa Fluor™ 488. From figure 11A and 11B, both collagens type I and III were highly expressed in the tissue sections. CN3-biotin was again observed all over the cells, yet it showed colocalization with the collagen. Enlargement of certain areas could clearly identify overlap between CN3-biotin and both collagens, as indicated by the magenta arrows. From observations, it appeared that the peptide colocalizes better with collagen type III, but as this could not been quantified these results should be handled with care.

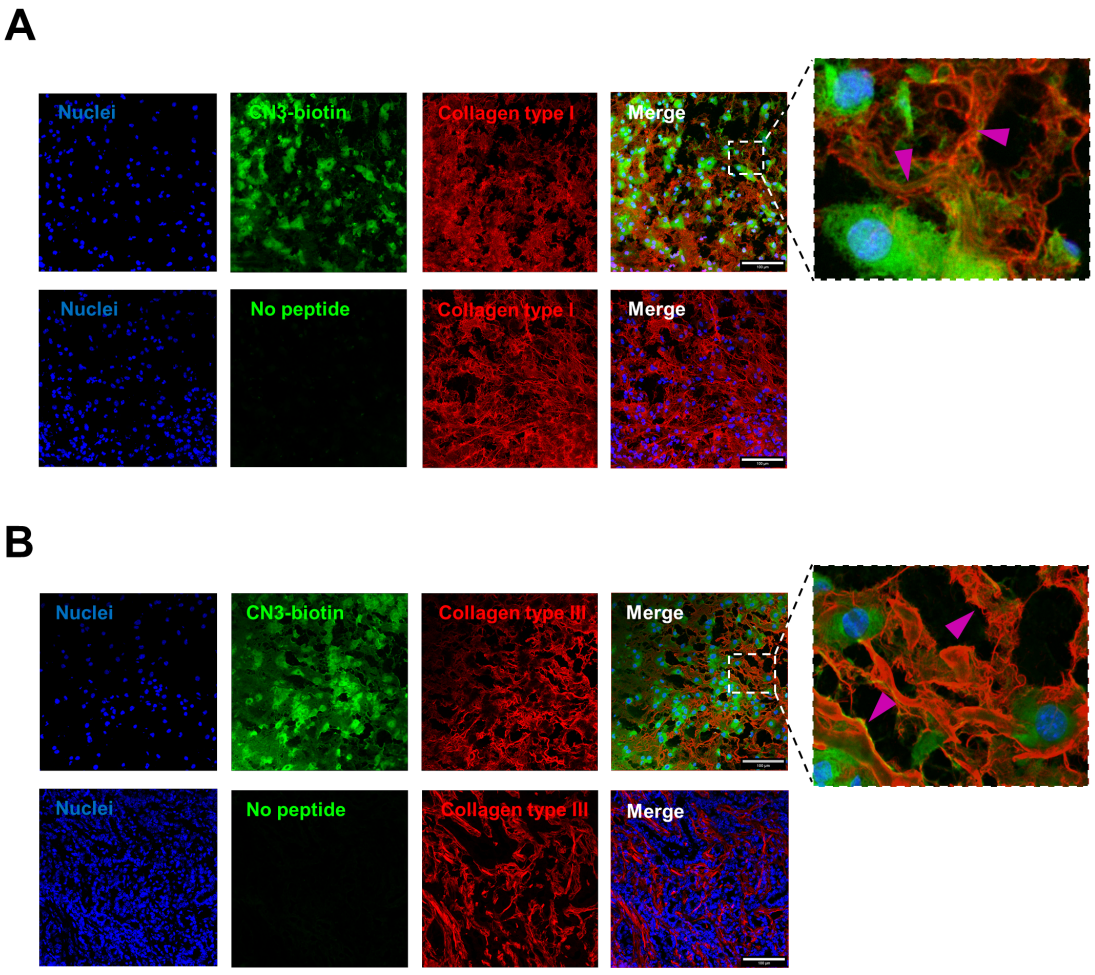

Figure 11: Immunofluorescence of KPC tumor tissue sections. A) Staining of tissue sections with 4′,6-diamidino-2-phenylindole (DAPI, blue), CN3-biotin (green), and goat anti-collagen type I (red). B) Staining of deposited collagen by hPaSteCs with 4′,6-diamidino-2-phenylindole (DAPI, blue), CN3-biotin (green), and goat anti-collagen type III (red). Representative images (n=2), scale bar = 100 μm.

3.6 Preparation and characterization of CN3-coupled liposomes

To fulfill the goal to deliver therapeutics and/or diagnostics to the TME, a carrier was needed. Here, liposomes were used due to the aforementioned characteristics. PEG- and DBCO-liposomes were synthesized according to the ethanol-injection method and extruded through multiple track-etched membranes with descending pore sizes [76]. The molar ratio of lipids and the extrusion-process of the DBCO-liposomes were optimized to obtain the desired size (table A1). Coupling of the CN3-peptide to the DBCO-liposomes was facilitated using copper-free click chemistry (SPAAC) (figure 12A). After 24 hours incubation, the coupling efficiency was determined by a self-developed method. In brief, a small part of the mixture containing CN3-coupled liposomes and free CN3-azide was diluted and ultracentrifuged immediately after coupling. Then, the absorbance of supernatant was measured, and the coupling efficiency was calculated using equation 2. The size, PDI, zetapotential, and coupling efficiency of the liposomes can be found in figure 12B.

3.6.1 Hydrodynamic size and zeta potential of CN3-liposomes

The size of the PEG-liposomes, which were used as a control for all experiments, were 113 ± 1 nm. The DBCO-liposomes had an average size of 112 ± 3 nm while the CN3-coupled liposomes had an average size of 171 ± 10 nm, indicating that the size increases when the DBCO-liposomes are interacting with the CN3-azide. Noteworthy, efforts were performed to optimize sCN3-liposomes. Yet, sCN3-liposomes kept measuring particle sizes over 1000 nm (data not shown). A representative distribution of PEG-, DBCO-, and CN3-liposomes can be found in figure A4.
In addition, the PDI, a measure ranging from 0 (low) to 1 (high) that describes the dispersity of the particle size distribution [80], was 0.09 ± 0.02 for the PEG liposomes, 0.17 ± 0.03 for the DBCO-liposomes, and 0.23 ± 0.01 for the CN3-coupled liposomes which indicated monodispersity of the samples. Measuring the potential of all liposomal solutions did not show any difference as the zetapotential was -10.4 ± 0.4 mV, -10.9 ± 0.8 mV, and -10.6 ± 0.5 mV for the PEG, DBCO, and CN3-coupled liposomes, respectively.
The coupling efficiency of the CN3-coupled liposomes was measured (figures 12B and A4) and calculated using equation 2. By taking the loss of the concentration liposomes after extrusion into account, the coupling efficiency was measured at 62.4 ± 12.6%, suggesting that CN3 has been successfully coupled to the liposomes.

3.6.2 Colloidal stability of CN3-liposomes

To research the colloidal stability of the liposomes for long-term storage, the DBCO-liposomes and the CN3-liposomes were measured for their size and PDI at fixed time points over the course of 56 days (figure 12C and 12D). As shown in figures 12C, the size of the DBCO-liposomes at day 0 was measured at 103 ± 1 nm while after 56 days the size was measured at 117 ± 1 nm. The PDI at day 0 was measured at 0.12 ± 0.01 and increased to 0.23 ± 0.01 in 56 days. Both parameters appeared to increase most rapidly in the first 14 days. Yet, only a slight increase in size and PDI over the course of 56 days indicate stability of the formulation.
In figure 12D, the stability of the CN3-liposomes is depicted. At day 0, the CN3-liposomes were measured at 152 ± 1 nm, while the size increased to 168 ± 3 nm in 56 days. The PDI increased from 0.16 ± 0.02 to 0.25 ± 0.01. The small increase in size and PDI over the course of 56 days indicate overall colloidal stability of the CN3-liposomes.

3.7 Binding of CN3-liposomes to collagen-coated plates

To examine binding of the CN3-liposomes to collagen type I and type III, a liposome binding assay was performed. In short, collagen types I and III were coated on an ELISA plate and blocked before red fluorescent CN3-liposomes were allowed to bind to the collagen with or without a 50-times molar excess of CN3-peptide. Then, unbound liposomes were washed off, DMSO was added to the wells, and the content of each well was transferred to a black plate to measure

fluorescent intensity. Collagen-coated wells incubated without any liposomes and with red fluorescent PEG-liposomes were used a control. The fluorescent intensity of the collagen-coated wells without liposomes was subtracted from the other values. Results of the binding assay can be found in figure 12E.

The CN3-liposomes showed a six-fold increase in binding to collagen type I (5.9 to 1, $p<0.001$) and a seven-fold increase in binding to collagen type III (6.6 to 1, $p<0.001$), indicating a slightly better binding to collagen type III. However, no statistically significant difference was observed for the CN3-liposomes between both collagens. Blocking the liposomes with excess CN3-peptide showed no statistically significant difference in collagen type I ($p = 0.2453$) while it did in collagen type III. However, it should be mentioned that in both individual experiments a statistically significant difference was observed between CN3-liposomes and 'blocked' for both types of collagens (data not shown). Interestingly, a 50-times molar excess of CN3-peptide did not seem to inhibit binding of the CN3-liposomes much which might indicate that there are still binding sites left for the individual peptides to bind to.

A

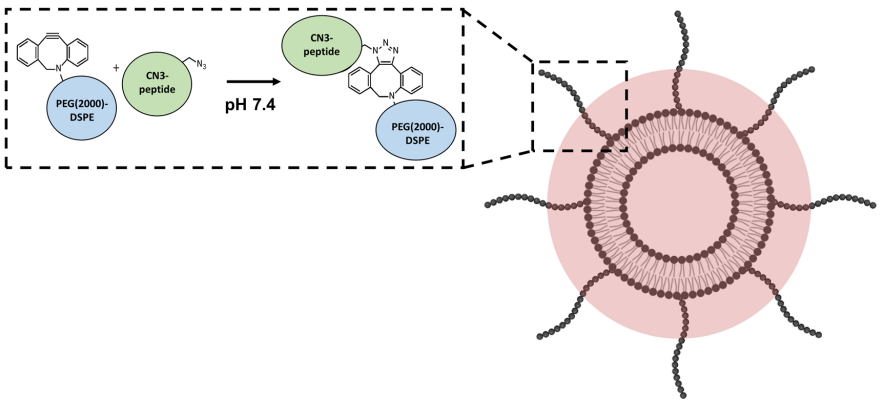

B

Liposomes	Size (nm)	PDI	Zetapotential (mV)	Coupling efficiency (%)
PEG	113 ± 1	0.09 ± 0.02	-10.4 ± 0.4	-
DBCO	112 ± 3	0.17 ± 0.03	-10.9 ± 0.8	-
CN3	171 ± 10	0.23 ± 0.01	-10.6 ± 0.5	62.4 ± 12.6

C

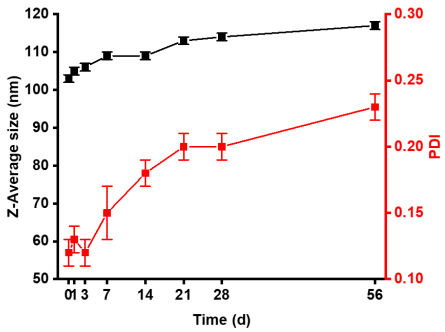

D

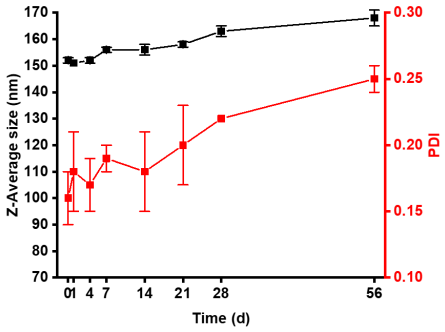

E

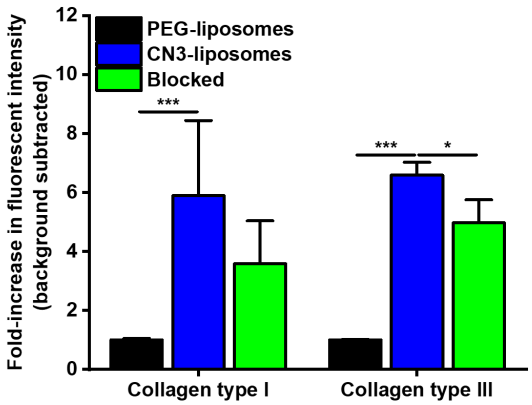

Figure 12: Preparation and characterization of CN3-coupled liposomes. A) Schematic representation of the liposomes and the coupling mechanism of dibenzocyclooctyl (DBCO) and azide-conjugated CN3-peptide. B) Characterization in terms of size, zetapotential, and PDI for the PEG- (n=6, 2 experimental replicates), DBCO-, and CN3-liposomes (n=9, 3 experimental replicates). For the CN3-liposomes, the coupling-efficiency is measured as well (n=6, 3 experimental replicates). C) Stability in terms of size and PDI for the DBCO-liposomes (n=3). D) Stability in terms of size and PDI for the CN3-liposomes (n=3). E) Quantification of the liposome binding assay on collagen types I and III for PEG-liposomes, CN3-liposomes, and CN3-liposomes with a 10-times molar excess of CN3-peptide (blocked) (n=6, 2 experimental replicates). Statistical analyses were done using analysis of variance (ANOVA). $*p<0.05$.; $***p<0.001$.

3.8 Cellular uptake of CN3-liposomes

To investigate whether the collagen-bound liposomes could be engulfed by phagocytic cells, a preliminary liposome uptake study was performed. In brief, tissue-culture treated 24-well plates were coated with collagen type I and blocked with 2% BSA. Then, red fluorescent CN3-liposomes were allowed to bind to the collagen and unbound liposomes were washed away afterwards. Collagen-coated wells incubated without any liposomes and with red fluorescent PEG-liposomes were used a control. To verify binding of the CN3-coupled liposomes, DMSO was added to certain wells after washing and the fluorescent intensity was measured as described in section 2.6.1.

From figure 13A, a seven-fold increase in fluorescent intensity was observed (6.8 to 1, $p<0.001$), indicating more binding of the CN3-liposomes to the collagen as compared to the PEG-liposomes. After washing the wells, hPaSteCs were added to the wells and incubated at 37°C overnight. Cellular uptake of the liposomes was analyzed using flow cytometry twice per well. The results can be found in figure 13.

The number of viable cells were measured to ensure equal comparison between groups. Approximately 10,000 cells were recovered from three wells (data not shown), indicating a low yield of cells. Gating the detected population revealed the live cells (figure 13B). The live cell population was approximately 66% of the total number of recovered cells, indicating a high fatality rate (data not shown). Although there was a slight increase in viable cells in the group containing the CN3-liposomes, this difference was not statistically significant ($p = 0.22211$).

Surprisingly, investigating the uptake of collagen-bound liposomes by hPaSteCs revealed an equal shift in peak in the fluorescent PE-A channel for both PEG and CN3-coupled liposomes, as compared to the group without any treatment. In figure 13D, the Mean Fluorescent Intensities of the gated populations are depicted. Consistent with figure 13C, hPaSteCs incubated with liposomes showed higher signal as compared the hPaSteCs without liposomes. Yet, no statistically significant difference was observed between no liposomes versus PEG liposomes ($p = 0.0745$), PEG-liposomes versus CN3 liposomes ($p = 0.2695$), and no liposomes versus CN3-liposomes ($p = 0.6999$). Results from 13C and 13D suggest improper uptake of both liposomes by hPaSteCs.

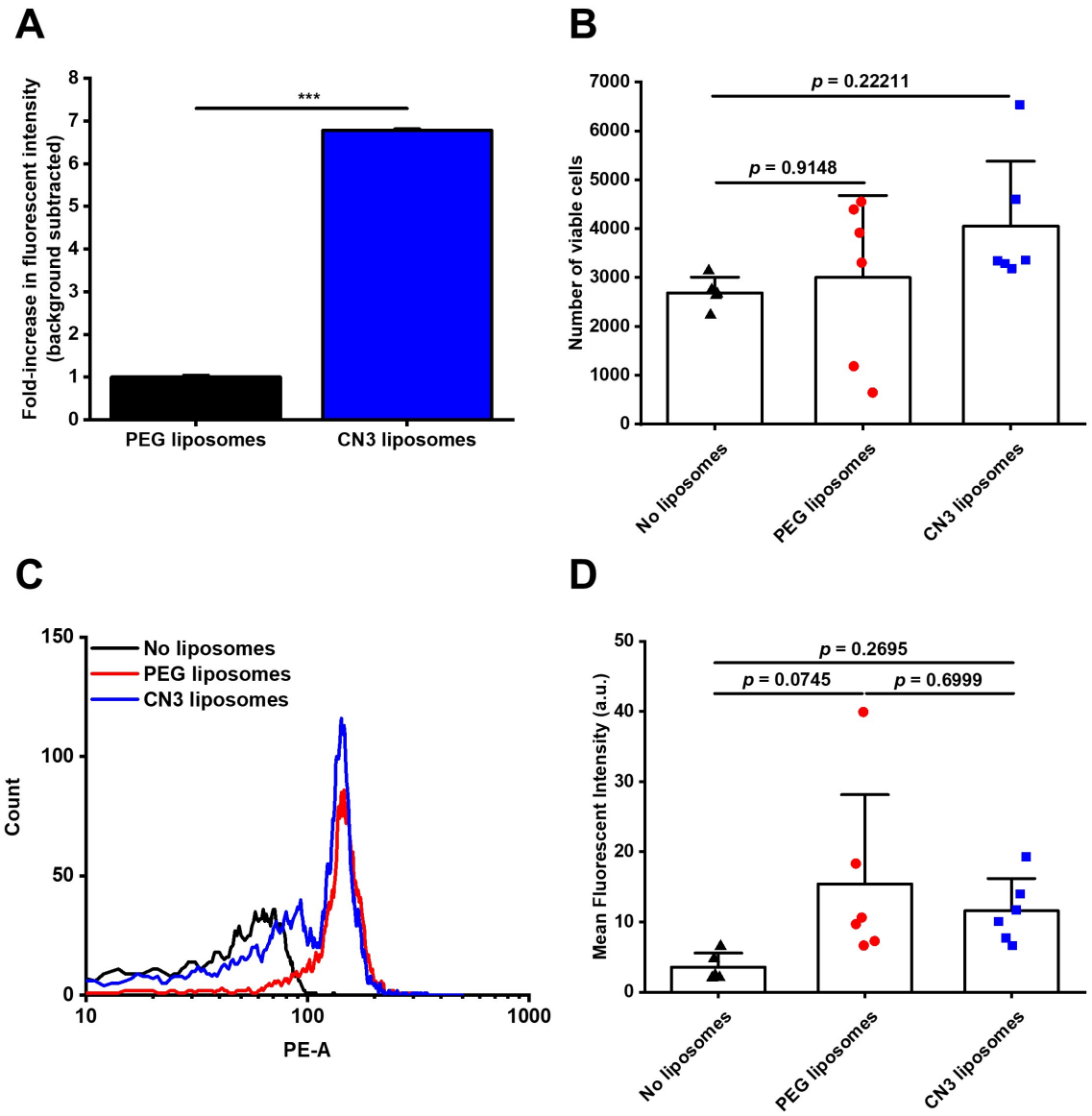

Figure 13: Quantification of the preliminary liposome uptake experiment. A) Comparison between PEG- and CN3-liposomes bound to the collagen type I-coated surface in terms of fluorescent intensity (n=2). B) Number of viable cells counted for no liposomes, PEG-liposomes, and CN3-liposomes (n=3, 2 measurements per sample). C) Count versus fluorescence of PE-A for no liposomes, PEG-liposomes, and CN3-liposomes, Representative measurements displayed. D) Mean Fluorescent Intensity in channel PE-A for no liposomes, PEG-liposomes, and CN3-liposomes (n=3, 2 measurements per sample). Statistical analyses were done using analysis of variance (ANOVA). $***p<0.001$.

4 Discussion

For the last decade, cancer research has been focusing on the tumor stroma and the number of published articles in which active targeting of the tumor stroma is discussed, has taken an immense leap. Hereby, targeting cell-surface receptors on different cells in the TME has been proven to be successful [81]. Nevertheless, this strategy requires the selection of specific cells of the TME and identifying specific cell-surface receptors for each type of cancer. In addition, targeting cells via specific receptors might induce drug resistance because of loss of receptors by mutation [82]. Therefore, targeting the most abundant structural protein within the fibrotic TME, namely collagen, could provide the establishment of a universal targeting strategy. By targeting collagens in the fibrotic TME, a reservoir of therapeutic agents can be created which could potentially enhance treatment of various cancers.
In this study, we identified and evaluated the novel CN3-peptide which showed increased affinity to collagen type III but also showed affinity to collagen type I. *In vitro* studies and staining of *ex vivo* KPC tissue sections demonstrated colocalization of the CN3-peptide with both collagen types I and III. The CN3-peptide could be coupled to liposomes, showed stability, and demonstrated increased binding to collagen type I and III as compared to controls. Uptake experiments exhibited no statistically significant difference between PEG-liposomes and CN3-liposomes.

The CN3-peptide showed binding to both fibrillar collagens type I and type III on the PEPspot™ membrane which is consistent with literature regarding binding of mannose receptors to collagens [70, 83]. The mannose receptor, from which the CN3-peptide is derived, can bind to native and fragmented collagen types I, III, and IV through the fibronectin type II domain [70]. Binding of the CN3-peptide to collagen type IV, which is regarded as the main collagen component of the basement membrane, was not evaluated. Yet, literature showed that collagen type IV is overexpressed in patients with PDAC and is mainly produced by the cancer cells themselves [84, 85]. Therefore, whether the CN3-peptide binds to collagen type IV might be interesting to investigate in future.

Comparison of peptide binding to both collagens was successfully evaluated using ELISAs. After trying various types of ELISAs and different conditions, a proper protocol was established and revealed that the CN3-peptide had a higher binding affinity towards collagen type III as compared to collagen type I. Furthermore, binding to collagen type II and fibronectin, another large ECM-protein [86], was rather low. In addition, binding of the CN3-biotin was successfully conducted by adding a 10- and 50-times molar excess of CN3-peptide.
Increased binding and inhibition was indicated by the overall higher absorbance values, indicating a greater antigen/peptide concentration [87], and, in comparing affinity to collagen type I and III, the differences in K_D-values in which a lower K_D-value implements stronger binding affinity [88]. The K_D-values were calculated by fitting the Hill equation to the data to determine ligand-receptor interactions, as described by Syedbasha *et al.* and Eble [89, 90]. The Hill coefficient, which may give information about interacting sites of the peptide with the protein [91], was set to 1 in all experiments. A Hill coefficient of 1 could mean either one-site-specific binding or multiple-site-binding without cooperativity. Furthermore, choosing a Hill coefficient of 1 opened the possibility to compare the data with the existing literature. However, it should be mentioned that the number of interacting sites is still unknown. Parameters of the Hill equation could be determined more exact by Surface Plasmon Resonance (SPR). SPR, a golden-standard regarding ligand-receptor interactions, is technique used to measure ligand-receptor interactions at real-time and can be used to reveal binding affinities and kinetics [92].
The calculated K_D-values for CN3-biotin showed moderate binding affinity as the values lay between 0.1 nM and 1 μM [93]. Having a moderate binding affinity, the peptide and peptide-conjugated moieties should be able to deeply penetrate tumors [58, 67]. In terms of the peptide size and binding affinity towards collagen type III, uniqueness of the CN3-peptide is highlighted when comparing to other studies that have used collagen type I and/or type III-binding

peptides. Hubbell *et al.* found their collagen-binding domain to have higher binding affinities as compared to CN3-biotin (1.8 nM and 40.6 nM for collagen type I and type III, respectively) [67]. However, as their collagen-binding domain has a molecular weight of 35 kDa compared to 1.2 kDa for the CN3-peptide, conjugation to, for instance, nanoparticles could be an issue. Liang and colleagues showed their peptide of 0.9 kDa having a binding affinity of 210 nM for collagen type I, which is comparable to the binding affinity of CN3-biotin to collagen type I [68]. More interestingly, the binding affinity of the mannose receptor and the fibronectin type II domain of the mannose receptor was evaluated by Napper and coworkers. Both the receptor and its specific domain showed the same binding affinity and was estimated at 4.2 ± 0.3 μM for collagen type I and 6.0 ± 1.4 μM for collagen type III [70]. This suggest that the CN3-peptide has a higher binding affinity to both collagens as compared to the receptor and its collagen-binding domain from which it is derived. Yet, Napper and colleagues used a different method to estimate the binding affinity which makes it hard to compare estimated binding affinities.

The CN3-biotin showed low to no binding to collagen type II, another type of fibrillar collagen [30]. Binding to fibronectin, which is also upregulated in the fibrotic tumor stroma [94], showed low signal as well, emphasizing specificity of the CN3-peptide to collagen types I and III. However, binding to other common proteins, with various properties, of the fibrotic TME was not evaluated which is a limitation of the experiment.

Regarding the studies in which the CN3-biotin was blocked with a 10- and 50-times molar excess of CN3-peptide, indication of specific binding was observed [89]. Yet, one might expect greater inhibition of the signal when using a 50-times molar excess of CN3-peptide. This could be explained by unoccupied binding sites on the collagen which might suggest that the peptide is able to bind to multiple sites on the collagen. The latter could be reason to change the Hill coefficient used when calculating the K_D-values in ELISA [91].

A possible binding mechanism which drives binding of the CN3-peptide to the collagens could be related to the hydrophobic properties of the peptide. Collagen types I and III have been found to display hydrophobic pockets or 'grooves' to which hydrophobic side chains of the CN3-peptide could possibly bind to [95, 96]. Hu and colleagues proposed a similar mechanism for the binding of the fibronectin type II domain to collagen and revealed that binding to collagen might depend on pH, degree of glycosylation, and concentration of calcium-ions [96]. In addition, since the CN3-peptide contains a cysteine residue, there is a possibility that the peptide can form disulfide bridges, which are strong, covalent interactions, when binding to its specific site on the collagen [97]. Regarding the differences between the evaluated collagen types, the fibril diameter of collagen type III is smaller as compared to collagen type I. Birk *et al.* concluded that collagen type III probably has more charged and hydrophobic regions as compared to collagen type I, resulting in the difference in fibril diameter [95]. The latter study also showed that collagen type II had smaller fibril diameters as compared to collagen type III which suggests that collagen type II has even more hydrophobic and charged regions [95]. Yet, the extent of fibril formation, which could determine the eventual fibril structure, was lower for collagen type II as compared to collagen type III. Referring to the ELISA in which collagen type II was coated as well, the CN3-peptide did hardly show any binding. This indicates that the CN3-peptide probably undergoes more, or even different, interactions with collagen type III as proposed and are yet to be explored. As a major limitation, experiments in which CN3-biotin is blocked, were not conducted with collagen type I, collagen type II, nor fibronectin. The latter could give more information binding properties of the CN3-peptide.

In vitro binding experiments demonstrated that collagen types I and III were produced by TGF-β1-activated hPaSteCs and CN3-biotin appeared all over the cells. CN3-biotin did show colocalization with both collagens and had a greater value for collagen type III. Using a 10-times molar excess of CN3-peptide, the fluorescence of CN3-biotin was significantly reduced.

TGF-β1, a common factor to increase the α-smooth muscle actin (α-SMA) protein in fibroblasts, was used to enhance fibroblast-to-myofibroblast differentiation in hPaSteCs [98]. Myofibroblasts have increased collagen type I and collagen

type III production and this effect was also demonstrated by stimulating hPaSteCs with TGF-β1 [99, 100]. A higher concentration of collagen type I as compared to collagen type III is observed in patients, as well as in cultured hPaSteCs [101, 100, 102]. In addition, the produced collagen remained intracellular which is common in two-dimensional cultures of hPaSteCs [101].

Although the cells were fixed with acetone/methanol, which is known to permeabilize the cell membrane, CN3-biotin appeared all over the hPaSteCs and not just on the collagen. In search for a proper negative control, a similar pattern of green signal was observed in KPC cells. Since there was no collagen present in the KPC cells and the green fluorescence was observed everywhere, it was suggested that CN3-biotin interacts with cells in a different way. By recalling the properties of the peptide, the CN3-peptide is largely hydrophobic and has a net charge of +1 at pH 7.0. Therefore, a possible explanation is that the peptide interacts with the cell membrane as shown by many using antimicrobial peptides [103, 104, 105]. More precise, the higher the hydrophobicity of a peptide, the deeper the peptide will penetrate the lipid bilayer of the cell membrane [104]. The small positive charge could interact with the negatively charged headgroups of the phospholipids [104]. Considering the CN3-peptide was conjugated to biotin using a hydrophilic PEG(6)-spacer, the CN3-peptide could penetrate the lipid bilayer while PEG(6)-biotin is then displayed on the extracellular side of the lipid bilayer.

The Pearson correlation coefficient r was used to determine colocalization between the fluorescence coming from the CN3-biotin and either collagen type I or type III. The Pearson correlation coefficient r describes pixel correlation between fluorophores and is a number between -1 and +1. A coefficient of -1 means perfect but negative correlation, 0 means no correlation, and +1 means perfect positive correlation [106]. Mander's overlap coefficient has been used to quantify colocalization in literature as well. However, since Mander's overlap coefficient is hard to interpret and favors high intensity combinations, the use of Pearson correlation coefficient r is regarded as the golden-standard [106].

A high degree of colocalization was observed for both types of collagens. Yet, the colocalization of CN3-biotin with collagen type III was greater as compared to collagen type I. Unfortunately, the expression of collagen type III was low which could hamper the comparison of colocalization.

In a slightly different *in vitro* experiment, hPaSteCs were subjected to TGF-β1 and Dextran Sulfate. This resulted in an increase in deposition of collagen type I, but not in collagen type III. CN3-biotin appeared all over the cells in both treated and non-treated samples. Colocalization was visualized and revealed a high degree of colocalization, especially in collagen type III. However, unspecific signal contributed to this difference. Interestingly, the signal of CN3-biotin was significantly increased in treated samples, as compared to non-treated samples.

Deposition of collagen is a multi-steps process and requires upregulation of certain enzymes to execute post-translational modification of the collagen [11]. There is, however, a short-cut to facilitate collagen deposition *in vitro*. The use of Dextran Sulfate (DxS) 500 kDa in ECM-producing cells has been demonstrated by many [107, 108, 109]. DxS has a similar structure to natural glycosaminoglycans and can bind to cytokines, such as TGF-β1 [108]. Furthermore, DxS has shown to enhance growth factor-mediated signaling, including signaling of TGF-β1 [110]. In search for the mechanism of DxS, it was believed that collagen deposition was promoted by the macromolecular crowding effect [109, 111]. A recent study has shown that collagen deposition is promoted by aggregation of negatively charged DxS with collagen and fibronectin [108].

Since DxS was found to enhance TGF-β1-mediated signaling and collagen deposition, it was expected that, when incubating the samples with both TGF-β1 and DxS, the expression both collagen type I and III should increase. The latter was indeed the case for collagen type I, as described in literature [108], but not for collagen type III which is a major limitation of the model. From literature, using DxS with and without TGF-β1 did not result in an increased collagen type III deposition, as compared to negative controls and other macromolecules known to enhance collagen deposition [112, 113]. Using longer incubation times and cultures with low amounts of serum, did not enhance collagen

type III production but rather in a decreased cell viability.
As demonstrated by the ELISAs, the CN3-peptide has affinity to collagen type I. Therefore, the experiment was continued with CN3-biotin. Like the previous *in vitro* experiment, CN3-biotin appeared all over the cells, but a certain degree of CN3-biotin was found on the deposited collagen fragments. Yet, certain collagen fragments, positioned away from the cells, did not show colocalization which could be a result of the collagen having an aberrant pattern as a results of DxS [113]. A high degree of colocalization was observed for both types of collagens. However, as shown by the samples without peptide, there was no deposition of collagen type III while the Pearson correlation coefficient r was close to +1. As the pattern of the green channel overlapped with the red channel in samples stained for collagen type III, it was clear that there might be channel leaking. Channel leaking, also known as bleed-through, is known to negatively affect reliability of colocalization measurements [79]. Referring to the excitation and emission spectra of AlexaFluor™ 488 and AlexaFluor™ 594, it becomes clear that the emission spectrum of AlexaFluor™ 488 overlaps with the excitation spectrum of AlexaFluor™ 594.
CN3-biotin revealed increased signal intensity when the samples were treated with both TGF-β1 and DxS. Since formaldehyde fixation is speculated to slightly destruct the integrity of the cell membrane, it could be possible that small molecules, like CN3-biotin, can enter the cell while antibodies cannot [114]. Yet, the earlier described mechanism in which the CN3-peptide could interact with the cell membrane is still plausible since fibroblasts are known to increase in size and spread out more when activated [115]. Removing cells before staining could be an interesting approach to avoid unspecific binding of the CN3-peptide [116].

Staining of *ex vivo* sections was conducted by using a genetically engineered mouse model of pancreatic cancer [75]. The model showed high amounts of matured and fibrillar collagen type I and collagen type III which made it more suitable for staining as compared to the *in vitro* models.
CN3-biotin was observed in proximity of the nuclei. However, CN3-biotin was also found near both collagens and colocalization of CN3-biotin with both collagens was observed. It appeared that CN3-biotin showed better colocalization with collagen type III, which is consistent with the previous data. Quantification of colocalization and the use of consecutive tissue sections would strengthen the analysis. In addition, injecting mice with fluorescent labeled CN3-peptide could provide more information. When injecting the mice, the CN3-peptide could bind to the collagen before fixation of the tissue sections. Fixation is known for damaging the tissue sections and could give skewed results [117].

The appealing properties of liposomes, as stated in section 1.7, make these type of nanocarriers good candidates for active targeted drug delivery. Yet, rapid clearance of these particles by the reticuloendothelial system make them vulnerable. Therefore, certain surface modifications are necessary to extent their circulation time *in vivo*. By using hydrophilic polymers, such as PEG, this circulation time can be extended [72].
Characterization of the produced PEG-, DBCO- and CN3-liposomes revealed a size increase for the CN3-liposomes. Stability tests showed a minor change in size and PDI. The coupling efficiency was measured at an average 62.4 ± 12.6%. Binding studies showed increased fluorescent signal as compared to controls.
In vivo passive targeting using the EPR-effect is most effective when nanoparticles have hydrodynamic diameters between 100 and 400 nm, which is in the range of the produced CN3-liposomes [118]. Yet, the EPR effect is highly heterogenous phenomenon and is known to be much larger in rodents as compared to humans [119]. Therefore, the produced CN3-liposomes might give difficulties when administered to humans. In addition, the increase in size of approximately 60 nm for the CN3-liposomes is not solely due to the peptide. The peptide has an approximate size of 0.42 nm, which adds, in theory, 0.84 nm to the diameter of the DBCO-liposomes. A possible explanation for the size increase could be fusion, swelling, and aggregation of the liposomes which can be induced by peptides [120].

Nonetheless, a slight negative charge on the liposomes could prevent aggregation and could have beneficial uptake properties while not being toxic to cells [121].
Coupling of the CN3-peptide to the liposomes was facilitated using strain-promoted alkyne-azide cycloaddition (SPAAC), a type of copper-free click chemistry [122]. DBCO-liposomes were coupled to azide-conjugated CN3-peptide at physiological pH [123, 122]. Noteworthy, although the DBCO-liposomes were stable over the course of 56 days, it did not mean that the liposomes could still be used for coupling. Gai and coworkers demonstrated that the DBCO-molecules per liposome decreased by more than 50% in the first week and it was suggested that the hydrophobic DBCO buries itself in the hydrophobic lipid bilayer over time [123].
The coupling-efficiency was calculated by measuring the absorbance of the supernatant after centrifugation of CN3-liposomes with free CN3-azide. For protein/peptide analysis, the most frequently used wavelength for detection is 280 nm. At 280 nm, aromatic amino acids tryptophan and tyrosine absorb the UV light [124]. Since our peptide does not contain any tryptophan and tyrosine, absorbance at a wavelength of 205 nm was detected. The absorbance between 180 and 230 nm is solely due to peptide-bonds [125]. Based on the developed equation (equation 2), the coupling-efficiency can never reach 100% as the DBCO-molecules are situated inwards as well as outwards of the liposomes. A perfect coupling-efficiency holds a number from 50% and above. An exact measurement of the coupling-efficiency should include measuring the availability of unbound DBCO on the liposomes, as proposed by Gai and colleagues [123], after coupling.

PEG-liposomes were used as a negative control for the liposome binding experiments and the uptake experiments. A similar study demonstrated the use of a scrambled version of the main peptide which functioned as a control [126]. A scrambled peptide displays the same sequence of amino acids, however, arranged in a different order as compared to the main peptide. Therefore, the lack of a scrambled version of the CN3-peptide, which could be coupled to the liposomes, is a limitation of the binding experiments.
Regarding the comparison of fluorescent intensities in the liposome binding experiments, one might expect a higher degree of binding of CN3-liposomes to both collagens as compared to the negative control. As discussed before, since the coupling efficiency did not include a measurement of the available DBCO-molecules, it is uncertain where the peptide ends up. In addition, if large amounts peptide gets buried in the lipid bilayer and only a small part is available for binding, one can expect an impairment of potential binding affinity [104, 123]. Using a 50-times molar excess of free CN3-peptide to block binding of the liposomes, only a small difference was observed which was not statistically significant in the combined measurements on collagen type I. A possible explanation could be that when CN3-liposomes bind, the free CN3-peptides are sterically hindered by these liposomes which make them unable to bind to the coated collagen [127]. The use of non-fluorescent CN3-liposomes to block the red fluorescent CN3-liposomes could be a better strategy. Yet, Ai and coworkers did manage to block liposomes with free peptide by pre-treating the collagen-coated plates with free peptide [61]. Thus, not pre-blocking the collagen-coated plates and not using proper controls are both major limitations of these binding experiments.

In a preliminary uptake experiment, hPaSteCs showed equal uptake of PEG- and CN3-liposomes. Yet, this difference was not statistically significant to the cells on collagen-coated surfaces without liposomes. Fibroblasts have shown to adhere to collagen type I within 2 hours and slowly spread afterwards [128, 129]. Regarding phagocytic behavior, quiescent hPaSteCs are known to act as phagocytic cells in the pancreas and is essential in limiting the extent of inflammation [130].
A low number of hPaSteCs (5,000 cells per well) was used to ensure a higher positive signal per cell when engulfing liposomes that were bound to the collagen. As a total of 15,000 cells were supposed to be counted per measurement, only 10,000 cells could be recovered from which 66% was indicated as viable.

Counting approximately 5,000 cells per measurements, which is regarded as low, had its effect on the measured fluorescent intensity [131]. Since the histograms revealed a ragged appearance and the count was rather low, the statistics were regarded as questionable. Since CN3-liposomes revealed an overall higher fluorescent intensity on the collagen-coated plates, it was expected that hPaSteCs in that group would contain an overall higher fluorescent intensity. Yet, the detected mean fluorescent intensities fluctuated a lot and did not reveal any statistically significant difference between samples. A possible explanation could be that the liposomes or peptides were degraded over time at physiological conditions in culture medium. The stability of the liposomes was not evaluated at those condition.
Another explanation for the low fluorescent signal observed, could be that the phagocytic activity of hPaSteCs was overestimated. Not much is known about the phagocytic activity of hPaSteCs. Stellate cells of the liver (HSCs) have been researched for their phagocytic behavior in quiescent state which could be applicable to hPaSteCs as well [132, 133]. Regarding the possible role of collagen type I, HSCs cultured on collagen type I gels stimulated activation of these cells which might alter the phagocytic behavior [134].
In an interesting review written by McKleroy *et al.*, it was discussed that collagen is degraded by MMPs, Cathepsin K, and by spontaneous denaturation and that these collagen fragments could be engulfed by fibroblasts [135]. Since the amount of collagen used in these experiments is rather high, it could be possible that the hPaSteCs were saturated with collagen fragments before engulfing fragments that include collagen-bound particles. In this regard, increasing the cell number could solve this problem. Yet, this does not explain the difference between PEG-liposomes and CN3-liposomes.

5 Conclusion

Targeting collagen in the tumor stroma could provide a novel approach to target desmoplastic adenocarcinomas.
This study demonstrated increased binding of the novel CN3-peptide to collagen type III as compared to collagen type I. Furthermore, neglectable binding to collagen type II and fibronectin was observed, indicating the specificity of the CN3-peptide to the collagens that are upregulated in the tumor stroma of adenocarcinomas. However, more proteins which could interact with the peptide were not evaluated.
Then, the CN3-peptide showed colocalization with collagen types I and III *in vitro*. Yet, collagen type III production was low as compared to collagen type I and the CN3-peptide was observed to bind unspecifically as well, which could be a result of its hydrophobicity.
Using PDAC tissue section from KPC mice, increased amounts of matured and fibrillar collagen types I and III was present as compared to *in vitro* experiments. Although the CN3-peptide appeared all over the cells, clear overlap was observed for both collagens which suggests that the CN3-peptide can bind to PDAC-induced native collagen types I and III.
In the search for collagen-binding nanoparticles, the CN3-peptide was coupled to liposomes and revealed high coupling-efficiencies which was measured using a self-developed method. Nevertheless, whether the hydrophobic CN3-peptide is encapsulated in the lipid bilayer or displayed on the exterior of the liposomes, remains unknown.
CN3-coupled liposomes showed great stability over time and demonstrated binding to collagen types I and III in a binding assay. Furthermore, although the CN3-liposomes could be blocked with excess free peptide, the inhibition of binding was low which could be due to steric hindrance of the liposomes.
Evaluating uptake of CN3-coupled liposomes, which were bound to collagen, showed no difference between CN3-coupled liposomes and control liposomes. Yet, the low cell count and choice of cells could have hampered the experiment. In addition, the stability of the liposomes at physiological conditions was not evaluated and could have its impact on the experiment as well.
Since the CN3-peptide did already show specific binding to collagen type I and collagen type III, further research should focus on improving the peptides' properties and binding specificity; evaluating different nanocarriers and their stability at physiological conditions; the choice and the ability to load therapeutic agents in the nanocarriers; improving *in vitro* models to evaluate binding, penetration, toxicity, and therapeutic efficacy of CN3-coupled nanocarriers; and performing *in vivo* distribution, toxicity, and efficacy studies.
All in all, this study demonstrated the use of the novel CN3-peptide to actively target collagen types I and III which are both known to be abundantly expressed in the fibrotic TME.

6 Future perspectives

Suggestions for future research were briefly mentioned in the conclusion. In this section, a more elaborate discussion on these ideas is provided.
At first, future research should focus on the properties and the binding specificity of the CN3-peptide. When binding of the CN3-peptide was visualized in *in vitro* and *ex vivo* experiments, it became clear that the CN3-peptide had some unspecific binding to the cells. As unspecific binding was not observed in ELISAs, the question arose what the possible mechanism could be. By searching for the properties of the CN3-peptide, the CN3-peptide showed to be largely hydrophobic and had hardly any charge. Therefore, it was suggested that the CN3-peptide could interact with the cell membrane or other hydrophobic molecules which should be investigated.
More difficulties were encountered when coupling the CN3-peptide to liposomes. As the binding affinity of the CN3-coupled liposomes was low, the above proposed phenomenon might be happening as well. Therefore, one should focus

on improving characteristics of the CN3-peptide by, for instance, adding or interchanging amino acids. Interchanged amino acids should contain increased charge or increased hydrophilicity that could possibly reduce unwanted effects. Furthermore, cyclization of the CN3-peptide might increase binding affinity and specificity as well. A better binding affinity and specificity was observed when producing cyclic RGD-peptides as compared to the linear versions of RGD-peptides [136]. A combination of the latter named modifications could result in a peptide with higher binding affinity and specificity.
In addition, selecting the right nanocarrier could solve the earlier named problems as well. By using nanocarriers that have more hydrophilic properties, one could prevent hydrophobic interactions of the peptide with the nanocarrier. The use of polymers to produce nanocarriers, such as poly (lactic-co-glycolic acid) (PLGA), allow tunability of the nanocarriers as one can vary the LA/GA-ratio to tune hydrophilicity [137]. Another benefit of using polymers is that the peptide can be coupled to the polymers before synthesizing the nanoparticles. Furthermore, as polymeric nanocarriers are more likely to appear as a network instead of a capsule, interactions such as those observed with hydrophobic peptides and lipid bilayers are undone.

After finding the right nanocarrier that allows the CN3-peptide to bind to the collagen to its full extend, one must thoroughly research the stability of the carriers at physiological conditions. Thereafter, one must determine which therapeutic agent to use in further experiments.

Improving *in vitro* models to evaluate binding, penetration, toxicity, and therapeutic efficacy of CN3-coupled nanocarriers is another aspect for future research. The current study has shown that two-dimensional cultures of activated hPaSteCs did not result in the desmoplastic reaction observed *in vivo*. Three-dimensional *in vitro* models in which fibroblasts are activated and in which high expression of collagen types I and III is observed, could be interesting to use [138, 139]. In such a model, one can evaluate binding and penetration of the nanocarriers. The penetration depth of the nanocarriers could reveal whether this approach is substantial or not, as demonstrated in a study performed by Ai *et al.* [61].

All the existing studies that have used collagen-binding moieties, proceeded to *in vivo* rather quickly. After experiments that demonstrated binding characteristics of their collagen-binding moiety, the moiety was coupled to a therapeutic agent or a carrier, and was then injected in mice [61, 65, 66, 67, 68, 69]. Since the tissue sections provided a lot of information and showed high amounts of collagen, injecting KPC mice with fluorescent-labeled CN3-coupled nanocarriers could give more information about the distribution and penetration of CN3-coupled nanocarriers.

7 Acknowledgements

I would like to thank prof. dr. Jai Prakash for his support and his assistance during my time at the Engineered Therapeutics group. Together, we came with many ideas, and I feel like we had some good dynamic. Thereby, I am grateful that we could write a book chapter together and that you have invited me to join the organizing-committee of the NanoTME 2021 conference. I have learned a lot from that.
Furthermore, I would like to thank Ahmed Mostafa, MSc and Kunal Pednekar, MSc for teaching me many techniques and for their assistance in certain experiments. Moreover, I would like to thank Marcel Heinrich, MSc for the critical evaluation of my report and the feedback he provided. Thereafter, I thank Hetty ten Hoopen, Lydia Bolhuis-Versteeg, Kirsten van Leijenhorst-Groener, Regine van der Hee, Cindy Huiskes, Tom Knop, and Ine Segers-Nolten for their great technical assistance. I would like to thank prof. dr. Marcel Karperien and dr. ir. Jeroen Rouwkema for being part of my committee and evaluating my work. Furthermore, I would like to thank Lisanne Morshuis, MSc; dr. Jan

Hendriks, and Niels Willemen, MSc for providing materials to complete certain experiments. Finally, I would like to thank the whole AOT-ET group for the great times and all the support.

References

[1] Sahai E, Astsaturov I, Cukierman E, DeNardo DG, Egeblad M, Evans RM, et al. A framework for advancing our understanding of cancer-associated fibroblasts. Nature Reviews Cancer. 2020 Jan;20(3):174–186. Available from: https://doi.org/10.1038/s41568-019-0238-1.

[2] Sung H, Ferlay J, Siegel RL, Laversanne M, Soerjomataram I, Jemal A, et al. Global Cancer Statistics 2020: GLOBOCAN Estimates of Incidence and Mortality Worldwide for 36 Cancers in 185 Countries. CA: A Cancer Journal for Clinicians. 2021 Feb;71(3):209–249. Available from: https://doi.org/10.3322/caac.21660.

[3] Siegel RL, Miller KD, Jemal A. Cancer statistics, 2020. CA: A Cancer Journal for Clinicians. 2020 Jan;70(1):7–30. Available from: https://doi.org/10.3322/caac.21590.

[4] Hanahan D, Weinberg RA. Hallmarks of Cancer: The Next Generation. Cell. 2011 Mar;144(5):646–674. Available from: https://doi.org/10.1016/j.cell.2011.02.013.

[5] Liu Y, Hu X, Han C, Wang L, Zhang X, He X, et al. Targeting tumor suppressor genes for cancer therapy. BioEssays. 2015 Oct;37(12):1277–1286. Available from: https://doi.org/10.1002/bies.201500093.

[6] TORRY DS, COOPER GM. Proto-Oncogenes in Development and Cancer. American Journal of Reproductive Immunology. 1991 Apr;25(3):129–132. Available from: https://doi.org/10.1111/j.1600-0897.1991.tb01080.x.

[7] Willis R. Targeted Cancer Therapy: Vital Oncogenes and a New Molecular Genetic Paradigm for Cancer Initiation Progression and Treatment. International Journal of Molecular Sciences. 2016 Sep;17(9):1552. Available from: https://doi.org/10.3390/ijms17091552.

[8] Whiteside TL. The tumor microenvironment and its role in promoting tumor growth. Oncogene. 2008 Oct;27(45):5904–5912. Available from: https://doi.org/10.1038/onc.2008.271.

[9] Wang M, Zhao J, Zhang L, Wei F, Lian Y, Wu Y, et al. Role of tumor microenvironment in tumorigenesis. Journal of Cancer. 2017;8(5):761–773. Available from: https://doi.org/10.7150/jca.17648.

[10] Balkwill FR, Capasso M, Hagemann T. The tumor microenvironment at a glance. Journal of Cell Science. 2012 Dec;125(23):5591–5596. Available from: https://doi.org/10.1242/jcs.116392.

[11] Henke E, Nandigama R, Ergün S. Extracellular Matrix in the Tumor Microenvironment and Its Impact on Cancer Therapy. Frontiers in Molecular Biosciences. 2020 Jan;6. Available from: https://doi.org/10.3389/fmolb.2019.00160.

[12] Xi KX, Wen YS, Zhu CM, Yu XY, Qin RQ, Zhang XW, et al. Tumor-stroma ratio (TSR) in non-small cell lung cancer (NSCLC) patients after lung resection is a prognostic factor for survival. Journal of Thoracic Disease. 2017 Oct;9(10):4017–4026. Available from: https://doi.org/10.21037/jtd.2017.09.29.

[13] Maitra A, Hruban RH. Pancreatic Cancer. Annual Review of Pathology: Mechanisms of Disease. 2008 Feb;3(1):157–188. Available from: https://doi.org/10.1146/annurev.pathmechdis.3.121806.154305.

[14] Conklin MW, Keely PJ. Why the stroma matters in breast cancer. Cell Adhesion & Migration. 2012 May;6(3):249–260. Available from: https://doi.org/10.4161/cam.20567.

[15] Flier JS, Underhill LH, Dvorak HF. Tumors: Wounds That Do Not Heal. New England Journal of Medicine. 1986 Dec;315(26):1650–1659. Available from: https://doi.org/10.1056/nejm198612253152606.

[16] Provenzano PP, Hingorani SR. Hyaluronan, fluid pressure, and stromal resistance in pancreas cancer. British Journal of Cancer. 2013 Jan;108(1):1–8. Available from: https://doi.org/10.1038/bjc.2012.569.

[17] Chandler C, Liu T, Buckanovich R, Coffman LG. The double edge sword of fibrosis in cancer. Translational Research. 2019 Jul;209:55–67. Available from: https://doi.org/10.1016/j.trsl.2019.02.006.

[18] Mammoto T, Jiang A, Jiang E, Panigrahy D, Kieran MW, Mammoto A. Role of Collagen Matrix in Tumor Angiogenesis and Glioblastoma Multiforme Progression. The American Journal of Pathology. 2013 Oct;183(4):1293–1305. Available from: https://doi.org/10.1016/j.ajpath.2013.06.026.

[19] Liu T, Han C, Wang S, Fang P, Ma Z, Xu L, et al. Cancer-associated fibroblasts: an emerging target of anti-cancer immunotherapy. Journal of Hematology & Oncology. 2019 Aug;12(1). Available from: https://doi.org/10.1186/s13045-019-0770-1.

[20] Casey T, Bond J, Tighe S, Hunter T, Lintault L, Patel O, et al. Molecular signatures suggest a major role for stromal cells in development of invasive breast cancer. Breast Cancer Research and Treatment. 2008 Mar;114(1):47–62. Available from: https://doi.org/10.1007/s10549-008-9982-8.

[21] Kalluri R. The biology and function of fibroblasts in cancer. Nature Reviews Cancer. 2016 Aug;16(9):582–598. Available from: https://doi.org/10.1038/nrc.2016.73.

[22] Boyd LNC, Andini KD, Peters GJ, Kazemier G, Giovannetti E. Heterogeneity and plasticity of cancer-associated fibroblasts in the pancreatic tumor microenvironment. Seminars in Cancer Biology. 2021 Mar. Available from: https://doi.org/10.1016/j.semcancer.2021.03.006.

[23] Sultana A, Zainab H, S. Stromal desmoplasia as a possible prognostic indicator in different grades of oral squamous cell carcinoma. Journal of Oral and Maxillofacial Pathology. 2019;23(3):338. Available from: https://doi.org/10.4103/jomfp.jomfp_136_19.

[24] Cirri P, Chiarugi P. Cancer-associated-fibroblasts and tumour cells: a diabolic liaison driving cancer progression. Cancer and Metastasis Reviews. 2011 Nov;31(1-2):195–208. Available from: https://doi.org/10.1007/s10555-011-9340-x.

[25] Tian C, Clauser KR, Öhlund D, Rickelt S, Huang Y, Gupta M, et al. Proteomic analyses of ECM during pancreatic ductal adenocarcinoma progression reveal different contributions by tumor and stromal cells. Proceedings of the National Academy of Sciences. 2019 Sep;116(39):19609–19618. Available from: https://doi.org/10.1073/pnas.1908626116.

[26] Nissen NI, Karsdal M, Willumsen N. Collagens and Cancer associated fibroblasts in the reactive stroma and its relation to Cancer biology. Journal of Experimental & Clinical Cancer Research. 2019 Mar;38(1). Available from: https://doi.org/10.1186/s13046-019-1110-6.

[27] Ricard-Blum S. The Collagen Family. Cold Spring Harbor Perspectives in Biology. 2010 Dec;3(1):a004978–a004978. Available from: https://doi.org/10.1101/cshperspect.a004978.

[28] Reilly DM, Lozano J. Skin collagen through the lifestages: importance for skin health and beauty. Plastic and Aesthetic Research. 2021 Jan;2021. Available from: https://doi.org/10.20517/2347-9264.2020.153.

[29] Boraschi-Diaz I, Wang J, Mort JS, Komarova SV. Collagen Type I as a Ligand for Receptor-Mediated Signaling. Frontiers in Physics. 2017 May;5. Available from: https://doi.org/10.3389/fphy.2017.00012.

[30] Lian C, Wang X, Qiu X, Wu Z, Gao B, Liu L, et al. Collagen type II suppresses articular chondrocyte hypertrophy and osteoarthritis progression by promoting integrin 1-SMAD1 interaction. Bone Research. 2019 Mar;7(1). Available from: https://doi.org/10.1038/s41413-019-0046-y.

[31] MR L, R L, D VS, L B. Decreased collagen ratio type I/III in association with hemorrhoidal disease. Journal of Translational Science. 2018;5(5). Available from: https://doi.org/10.15761/jts.1000278.

[32] Volk SW, Wang Y, Mauldin EA, Liechty KW, Adams SL. Diminished Type III Collagen Promotes Myofibroblast Differentiation and Increases Scar Deposition in Cutaneous Wound Healing. Cells Tissues Organs. 2011;194(1):25–37. Available from: https://doi.org/10.1159/000322399.

[33] Conrad GW. Synthesis of type III collagen by fibroblasts from the embryonic chick cornea. The Journal of Cell Biology. 1980 Mar;84(3):501–512. Available from: https://doi.org/10.1083/jcb.84.3.501.

[34] Blazejewski S, Preaux AM, Mallat A, Brocheriou I, Mavier P, Dhumeaux D, et al. Human myofibroblastlike cells obtained by outgrowth are representative of the fibrogenic cells in the liver. Hepatology. 1995 Sep;22(3):788–797. Available from: https://doi.org/10.1002/hep.1840220315.

[35] Shoulders MD, Raines RT. Collagen Structure and Stability. Annual Review of Biochemistry. 2009 Jun;78(1):929–958. Available from: https://doi.org/10.1146/annurev.biochem.77.032207.120833.

[36] Gao L, Orth P, Cucchiarini M, Madry H. Effects of solid acellular type-I/III collagen biomaterials on in vitro and in vivo chondrogenesis of mesenchymal stem cells. Expert Review of Medical Devices. 2017 Aug;14(9):717–732. Available from: https://doi.org/10.1080/17434440.2017.1368386.

[37] BRAZEL D, OBERBAUMER I, DIERINGER H, BABEL W, GLANVILLE RW, DEUTZMANN R, et al. Completion of the amino acid sequence of the alpha1 chain of human basement membrane collagen (type IV) reveals 21 non-triplet interruptions located within the collagenous domain. European Journal of Biochemistry. 1987 Nov;168(3):529–536. Available from: https://doi.org/10.1111/j.1432-1033.1987.tb13450.x.

[38] Ramshaw JAM, Shah NK, Brodsky B. Gly-X-Y Tripeptide Frequencies in Collagen: A Context for Host–Guest Triple-Helical Peptides. Journal of Structural Biology. 1998;122(1-2):86–91. Available from: https://doi.org/10.1006/jsbi.1998.3977.

[39] Ishikawa Y, Bächinger HP. A molecular ensemble in the rER for procollagen maturation. Biochimica et Biophysica Acta (BBA) - Molecular Cell Research. 2013 Nov;1833(11):2479–2491. Available from: https://doi.org/10.1016/j.bbamcr.2013.04.008.

[40] Pinnell SR. Induction of Collagen Synthesis by Ascorbic Acid. Archives of Dermatology. 1987 Dec;123(12):1684. Available from: https://doi.org/10.1001/archderm.1987.01660360122023.

[41] Carlson BM. Tissues. In: The Human Body. Elsevier; 2019. p. 27–63. Available from: https://doi.org/10.1016/b978-0-12-804254-0.00002-8.

[42] Mouw JK, Ou G, Weaver VM. Extracellular matrix assembly: a multiscale deconstruction. Nature Reviews Molecular Cell Biology. 2014 Nov;15(12):771–785. Available from: https://doi.org/10.1038/nrm3902.

[43] KADLER KE, HOLMES DF, TROTTER JA, CHAPMAN JA. Collagen fibril formation. Biochemical Journal. 1996 May;316(1):1–11. Available from: https://doi.org/10.1042/bj3160001.

[44] Tjin G, White ES, Faiz A, Sicard D, Tschumperlin DJ, Mahar A, et al. Lysyl oxidases regulate fibrillar collagen remodelling in idiopathic pulmonary fibrosis. Disease Models & Mechanisms. 2017 Nov;10(11):1301–1312. Available from: https://doi.org/10.1242/dmm.030114.

[45] Bonnans C, Chou J, Werb Z. Remodelling the extracellular matrix in development and disease. Nature Reviews Molecular Cell Biology. 2014 Nov;15(12):786–801. Available from: https://doi.org/10.1038/nrm3904.

[46] Kalluri R, Weinberg RA. The basics of epithelial-mesenchymal transition. Journal of Clinical Investigation. 2009 Jun;119(6):1420–1428. Available from: https://doi.org/10.1172/jci39104.

[47] Xu S, Xu H, Wang W, Li S, Li H, Li T, et al. The role of collagen in cancer: from bench to bedside. Journal of Translational Medicine. 2019 Sep;17(1). Available from: https://doi.org/10.1186/s12967-019-2058-1.

[48] Zhang H, Ding C, Li Y, Xing C, Wang S, Yu Z, et al. Data mining-based study of collagen type III alpha 1 (COL3A1) prognostic value and immune exploration in pan-cancer. Bioengineered. 2021 Jan;12(1):3634–3646. Available from: https://doi.org/10.1080/21655979.2021.1949838.

[49] Kauppila S, Stenbäck F, Risteli J, Jukkola A, Risteli L. Aberrant type I and type III collagen gene expression in human breast cancerin vivo. The Journal of Pathology. 1998 Nov;186(3):262–268. Available from: https://doi.org/10.1002/(sici)1096-9896(1998110)186:3<262::aid-path191>3.0.co;2-3.

[50] Kehlet SN, Sanz-Pamplona R, Brix S, Leeming DJ, Karsdal MA, Moreno V. Excessive collagen turnover products are released during colorectal cancer progression and elevated in serum from metastatic colorectal cancer patients. Scientific Reports. 2016 Jul;6(1). Available from: https://doi.org/10.1038/srep30599.

[51] Chen X, Song E. Turning foes to friends: targeting cancer-associated fibroblasts. Nature Reviews Drug Discovery. 2018 Nov;18(2):99–115. Available from: https://doi.org/10.1038/s41573-018-0004-1.

[52] Kanzaki R, Pietras K. Heterogeneity of cancer-associated fibroblasts: Opportunities for precision medicine. Cancer Science. 2020 Jul;111(8):2708–2717. Available from: https://doi.org/10.1111/cas.14537.

[53] Geng X, Chen H, Zhao L, Hu J, Yang W, Li G, et al. Cancer-Associated Fibroblast (CAF) Heterogeneity and Targeting Therapy of CAFs in Pancreatic Cancer. Frontiers in Cell and Developmental Biology. 2021 Jul;9. Available from: https://doi.org/10.3389/fcell.2021.655152.

[54] Irvine AF, Waise S, Green EW, Stuart B, Thomas GJ. Characterising cancer-associated fibroblast heterogeneity in non-small cell lung cancer: a systematic review and meta-analysis. Scientific Reports. 2021 Feb;11(1). Available from: https://doi.org/10.1038/s41598-021-81796-2.

[55] Danhier F, Feron O, Préat V. To exploit the tumor microenvironment: Passive and active tumor targeting of nanocarriers for anti-cancer drug delivery. Journal of Controlled Release. 2010 Dec;148(2):135–146. Available from: https://doi.org/10.1016/j.jconrel.2010.08.027.

[56] Raucher D. Tumor targeting peptides: novel therapeutic strategies in glioblastoma. Current Opinion in Pharmacology. 2019 Aug;47:14–19. Available from: https://doi.org/10.1016/j.coph.2019.01.006.

[57] Adams GP, Schier R, McCall AM, Simmons HH, Horak EM, Alpaugh RK, et al. High Affinity Restricts the Localization and Tumor Penetration of Single-Chain Fv Antibody Molecules. Cancer Research. 2001;61(12):4750–4755. Available from: https://cancerres.aacrjournals.org/content/61/12/4750.

[58] Scodeller P, Asciutto EK. Targeting Tumors Using Peptides. Molecules. 2020 Feb;25(4):808. Available from: https://doi.org/10.3390/molecules25040808.

[59] London N, Movshovitz-Attias D, Schueler-Furman O. The Structural Basis of Peptide-Protein Binding Strategies. Structure. 2010 Feb;18(2):188–199. Available from: https://doi.org/10.1016/j.str.2009.11.012.

[60] Katsumata K, Ishihara J, Mansurov A, Ishihara A, Raczy MM, Yuba E, et al. Targeting inflammatory sites through collagen affinity enhances the therapeutic efficacy of anti-inflammatory antibodies. Science Advances. 2019 Nov;5(11). Available from: https://doi.org/10.1126/sciadv.aay1971.

[61] Ai X, Duan Y, Zhang Q, Sun D, Fang RH, Liu-Bryan R, et al. Cartilage-targeting ultrasmall lipid-polymer hybrid nanoparticles for the prevention of cartilage degradation. Bioengineering & Translational Medicine. 2020 Sep;6(1). Available from: https://doi.org/10.1002/btm2.10187.

[62] Hu HY, Lim NH, Ding-Pfennigdorff D, Saas J, Wendt KU, Ritzeler O, et al. DOTAM Derivatives as Active Cartilage-Targeting Drug Carriers for the Treatment of Osteoarthritis. Bioconjugate Chemistry. 2015 Feb;26(3):383–388. Available from: https://doi.org/10.1021/bc500557s.

[63] Huizinga EG, van der Plas RM, Kroon J, Sixma JJ, Gros P. Crystal structure of the A3 domain of human von Willebrand factor: implications for collagen binding. Structure. 1997 Sep;5(9):1147–1156. Available from: https://doi.org/10.1016/s0969-2126(97)00266-9.

[64] Addi C, Murschel F, Crescenzo GD. Design and Use of Chimeric Proteins Containing a Collagen-Binding Domain for Wound Healing and Bone Regeneration. Tissue Engineering Part B: Reviews. 2017 Apr;23(2):163–182. Available from: https://doi.org/10.1089/ten.teb.2016.0280.

[65] Ishihara J, Ishihara A, Sasaki K, Lee SSY, Williford JM, Yasui M, et al. Targeted antibody and cytokine cancer immunotherapies through collagen affinity. Science Translational Medicine. 2019 Apr;11(487). Available from: https://doi.org/10.1126/scitranslmed.aau3259.

[66] Mansurov A, Ishihara J, Hosseinchi P, Potin L, Marchell TM, Ishihara A, et al. Collagen-binding IL-12 enhances tumour inflammation and drives the complete remission of established immunologically cold mouse tumours. Nature Biomedical Engineering. 2020 Apr;4(5):531–543. Available from: https://doi.org/10.1038/s41551-020-0549-2.

[67] Sasaki K, Ishihara J, Ishihara A, Miura R, Mansurov A, Fukunaga K, et al. Engineered collagen-binding serum albumin as a drug conjugate carrier for cancer therapy. Science Advances. 2019 Aug;5(8). Available from: https://doi.org/10.1126/sciadv.aaw6081.

[68] Liang H, Li X, Wang B, Chen B, Zhao Y, Sun J, et al. A collagen-binding EGFR antibody fragment targeting tumors with a collagen-rich extracellular matrix. Scientific Reports. 2016 Feb;6(1). Available from: https://doi.org/10.1038/srep18205.

[69] Deng H, Yang W, Zhou Z, Tian R, Lin L, Ma Y, et al. Targeted scavenging of extracellular ROS relieves suppressive immunogenic cell death. Nature Communications. 2020 Oct;11(1). Available from: https://doi.org/10.1038/s41467-020-18745-6.

[70] Napper CE, Drickamer K, Taylor ME. Collagen binding by the mannose receptor mediated through the fibronectin type II domain. Biochemical Journal. 2006 Apr;395(3):579–586. Available from: https://doi.org/10.1042/bj20052027.

[71] Karthivashan G, Ganesan P, Park SY, Lee HW, Choi DK. Lipid-based nanodelivery approaches for dopamine-replacement therapies in Parkinson's disease: From preclinical to translational studies. Biomaterials. 2020 Feb;232:119704. Available from: https://doi.org/10.1016/j.biomaterials.2019.119704.

[72] Mitchell MJ, Billingsley MM, Haley RM, Wechsler ME, Peppas NA, Langer R. Engineering precision nanoparticles for drug delivery. Nature Reviews Drug Discovery. 2020 Dec;20(2):101–124. Available from: https://doi.org/10.1038/s41573-020-0090-8.

[73] Beltrán-Gracia E, López-Camacho A, Higuera-Ciapara I, Velázquez-Fernández JB, Vallejo-Cardona AA. Nanomedicine review: clinical developments in liposomal applications. Cancer Nanotechnology. 2019 Dec;10(1). Available from: https://doi.org/10.1186/s12645-019-0055-y.

[74] Bolte S, Cordelières FP. A guided tour into subcellular colocalization analysis in light microscopy. J Microsc. 2006 Dec;224(Pt 3):213–232.

[75] Lee JW, Komar CA, Bengsch F, Graham K, Beatty GL. Genetically Engineered Mouse Models of Pancreatic Cancer: The KPC Model (LSL-Kras G12D/ LSL-Trp53 R172H/ Pdx-1-Cre), Its Variants, and Their Application in Immuno-oncology Drug Discovery. Current Protocols in Pharmacology. 2016 Jun;73(1). Available from: https://doi.org/10.1002/cpph.2.

[76] Gouda A, Sakr OS, Nasr M, Sammour O. Ethanol injection technique for liposomes formulation: An insight into development, influencing factors, challenges and applications. Journal of Drug Delivery Science and Technology. 2021 Feb;61:102174. Available from: https://doi.org/10.1016/j.jddst.2020.102174.

[77] Mastrotto F, Brazzale C, Bellato F, Martin SD, Grange G, Mahmoudzadeh M, et al. In Vitro and in Vivo Behavior of Liposomes Decorated with PEGs with Different Chemical Features. Molecular Pharmaceutics. 2020 Jan. Available from: https://doi.org/10.1021/acs.molpharmaceut.9b00887.

[78] Briuglia ML, Rotella C, McFarlane A, Lamprou DA. Influence of cholesterol on liposome stability and on in vitro drug release. Drug Delivery and Translational Research. 2015 Mar;5(3):231–242. Available from: https://doi.org/10.1007/s13346-015-0220-8.

[79] Kim D, Curthoys NM, Parent MT, Hess ST. Bleed-through correction for rendering and correlation analysis in multi-colour localization microscopy. Journal of Optics. 2013 Sep;15(9):094011. Available from: https://doi.org/10.1088/2040-8978/15/9/094011.

[80] Mudalige T, Qu H, Haute DV, Ansar SM, Paredes A, Ingle T. Characterization of Nanomaterials. In: Nanomaterials for Food Applications. Elsevier; 2019. p. 313–353. Available from: https://doi.org/10.1016/b978-0-12-814130-4.00011-7.

[81] Roma-Rodrigues C, Mendes R, Baptista P, Fernandes A. Targeting Tumor Microenvironment for Cancer Therapy. International Journal of Molecular Sciences. 2019 Feb;20(4):840. Available from: https://doi.org/10.3390/ijms20040840.

[82] Holohan C, Schaeybroeck SV, Longley DB, Johnston PG. Cancer drug resistance: an evolving paradigm. Nature Reviews Cancer. 2013 Sep;13(10):714–726. Available from: https://doi.org/10.1038/nrc3599.

[83] Madsen DH, Leonard D, Masedunskas A, Moyer A, Jürgensen HJ, Peters DE, et al. M2-like macrophages are responsible for collagen degradation through a mannose receptor–mediated pathway. Journal of Cell Biology. 2013 Sep;202(6):951–966. Available from: https://doi.org/10.1083/jcb.201301081.

[84] Öhlund D, Lundin C, Ardnor B, Öman M, Naredi P, Sund M. Type IV collagen is a tumour stroma-derived biomarker for pancreas cancer. British Journal of Cancer. 2009 Jun;101(1):91–97. Available from: https://doi.org/10.1038/sj.bjc.6605107.

[85] Öhlund D, Franklin O, Lundberg E, Lundin C, Sund M. Type IV collagen stimulates pancreatic cancer cell proliferation, migration, and inhibits apoptosis through an autocrine loop. BMC Cancer. 2013 Mar;13(1). Available from: https://doi.org/10.1186/1471-2407-13-154.

[86] Proctor RA. Fibronectin: A Brief Overview of Its Structure, Function, and Physiology. Clinical Infectious Diseases. 1987 Jul;9(Supplement_4):S317–S321. Available from: https://doi.org/10.1093/clinids/9.supplement_4.s317.

[87] Thiha A, Ibrahim F. A Colorimetric Enzyme-Linked Immunosorbent Assay (ELISA) Detection Platform for a Point-of-Care Dengue Detection System on a Lab-on-Compact-Disc. Sensors. 2015 May;15(5):11431–11441. Available from: https://doi.org/10.3390/s150511431.

[88] Kastritis PL, Bonvin AMJJ. On the binding affinity of macromolecular interactions: daring to ask why proteins interact. Journal of The Royal Society Interface. 2013 Feb;10(79):20120835. Available from: https://doi.org/10.1098/rsif.2012.0835.

[89] Syedbasha M, Linnik J, Santer D, O'Shea D, Barakat K, Joyce M, et al. An ELISA Based Binding and Competition Method to Rapidly Determine Ligand-receptor Interactions. Journal of Visualized Experiments. 2016 Mar;(109). Available from: https://doi.org/10.3791/53575.

[90] Eble JA. Titration ELISA as a Method to Determine the Dissociation Constant of Receptor Ligand Interaction. Journal of Visualized Experiments. 2018 Feb;(132). Available from: https://doi.org/10.3791/57334.

[91] Prinz H. Hill coefficients, dose–response curves and allosteric mechanisms. Journal of Chemical Biology. 2009 Sep;3(1):37–44. Available from: https://doi.org/10.1007/s12154-009-0029-3.

[92] Capelli D, Parravicini C, Pochetti G, Montanari R, Temporini C, Rabuffetti M, et al. Surface Plasmon Resonance as a Tool for Ligand Binding Investigation of Engineered GPR17 Receptor, a G Protein Coupled Receptor Involved in Myelination. Frontiers in Chemistry. 2020 Jan;7. Available from: https://doi.org/10.3389/fchem.2019.00910.

[93] Kastritis PL, Moal IH, Hwang H, Weng Z, Bates PA, Bonvin AMJJ, et al. A structure-based benchmark for protein-protein binding affinity. Protein Science. 2011 Feb;20(3):482–491. Available from: https://doi.org/10.1002/pro.580.

[94] Hu D, Ansari D, Zhou Q, Sasor A, Hilmersson KS, Andersson R. Stromal fibronectin expression in patients with resected pancreatic ductal adenocarcinoma. World Journal of Surgical Oncology. 2019 Feb;17(1). Available from: https://doi.org/10.1186/s12957-019-1574-z.

[95] Birk DE, Silver FH. Collagen fibrillogenesis in vitro: Comparison of types I, II, and III. Archives of Biochemistry and Biophysics. 1984 Nov;235(1):178–185. Available from: https://doi.org/10.1016/0003-9861(84)90266-2.

[96] Hu Z, Shi X, Yu B, Li N, Huang Y, He Y. Structural Insights into the pH-Dependent Conformational Change and Collagen Recognition of the Human Mannose Receptor. Structure. 2018 Jan;26(1):60–71.e3. Available from: https://doi.org/10.1016/j.str.2017.11.006.

[97] Wiedemann C, Kumar A, Lang A, Ohlenschläger O. Cysteines and Disulfide Bonds as Structure-Forming Units: Insights From Different Domains of Life and the Potential for Characterization by NMR. Frontiers in Chemistry. 2020 Apr;8. Available from: https://doi.org/10.3389/fchem.2020.00280.

[98] Hu B, Wu Z, Phan SH. Smad3 Mediates Transforming Growth Factor-–Induced -Smooth Muscle Actin Expression. American Journal of Respiratory Cell and Molecular Biology. 2003 Sep;29(3):397–404. Available from: https://doi.org/10.1165/rcmb.2003-0063oc.

[99] Zeltz C, Alam J, Liu H, Erusappan PM, Hoschuetzky H, Molven A, et al. 111 Integrin is Induced in a Subset of Cancer-Associated Fibroblasts in Desmoplastic Tumor Stroma and Mediates In Vitro Cell Migration. Cancers. 2019 Jun;11(6):765. Available from: https://doi.org/10.3390/cancers11060765.

[100] Schnittert J, Heinrich MA, Kuninty PR, Storm G, Prakash J. Reprogramming tumor stroma using an endogenous lipid lipoxin A4 to treat pancreatic cancer. Cancer Letters. 2018 Apr;420:247–258. Available from: https://doi.org/10.1016/j.canlet.2018.01.072.

[101] Schneider E, Schmid-Kotsas A, Zhao J, Weidenbach H, Schmid RM, Menke A, et al. Identification of mediators stimulating proliferation and matrix synthesis of rat pancreatic stellate cells. American Journal of Physiology-Cell Physiology. 2001 Aug;281(2):C532–C543. Available from: https://doi.org/10.1152/ajpcell.2001.281.2.c532.

[102] Willumsen N, Ali SM, Leitzel K, Drabick JJ, Yee N, Polimera HV, et al. Collagen fragments quantified in serum as measures of desmoplasia associate with survival outcome in patients with advanced pancreatic cancer. Scientific Reports. 2019 Dec;9(1). Available from: https://doi.org/10.1038/s41598-019-56268-3.

[103] Nielsen JE, Bjørnestad VA, Lund R. Resolving the structural interactions between antimicrobial peptides and lipid membranes using small-angle scattering methods: the case of indolicidin. Soft Matter. 2018;14(43):8750–8763. Available from: https://doi.org/10.1039/c8sm01888j.

[104] Chen Y, Guarnieri MT, Vasil AI, Vasil ML, Mant CT, Hodges RS. Role of Peptide Hydrophobicity in the Mechanism of Action of -Helical Antimicrobial Peptides. Antimicrobial Agents and Chemotherapy. 2007 Apr;51(4):1398–1406. Available from: https://doi.org/10.1128/aac.00925-06.

[105] Lomize AL, Pogozheva ID, Lomize MA, Mosberg HI. The role of hydrophobic interactions in positioning of peripheral proteins in membranes. BMC Structural Biology. 2007;7(1):44. Available from: https://doi.org/10.1186/1472-6807-7-44.

[106] Adler J, Parmryd I. Quantifying colocalization by correlation: The Pearson correlation coefficient is superior to the Mander's overlap coefficient. Cytometry Part A. 2010 Mar;77A(8):733–742. Available from: https://doi.org/10.1002/cyto.a.20896.

[107] Wan HY, Shin RLY, Chen JCH, Assunção M, Wang D, Nilsson SK, et al. Dextran sulfate-amplified extracellular matrix deposition promotes osteogenic differentiation of mesenchymal stem cells. Acta Biomaterialia. 2021 Dec. Available from: https://doi.org/10.1016/j.actbio.2021.11.049.

[108] Assunção M, Wong CW, Richardson JJ, Tsang R, Beyer S, Raghunath M, et al. Macromolecular dextran sulfate facilitates extracellular matrix deposition by electrostatic interaction independent from a macromolecular crowding effect. Materials Science and Engineering: C. 2020 Jan;106:110280. Available from: https://doi.org/10.1016/j.msec.2019.110280.

[109] Lareu RR, Arsianti I, Subramhanya HK, Yanxian P, Raghunath M. In VitroEnhancement of Collagen Matrix Formation and Crosslinking for Applications in Tissue Engineering: A Preliminary Study. Tissue Engineering. 2007 Feb;13(2):385–391. Available from: https://doi.org/10.1089/ten.2006.0224.

[110] Logeart-Avramoglou D, Huynh R, Chaubet F, Sedel L, Meunier A. Interaction of specifically chemically modified dextrans with transforming growth factor 1: potentiation of its biological activity. Biochemical Pharmacology. 2002 Jan;63(2):129–137. Available from: https://doi.org/10.1016/s0006-2952(01)00834-6.

[111] Ellis RJ. Macromolecular crowding: an important but neglected aspect of the intracellular environment. Current Opinion in Structural Biology. 2001 Feb;11(1):114–119. Available from: https://doi.org/10.1016/s0959-440x(00)00172-x.

[112] Gaspar D, Fuller KP, Zeugolis DI. Polydispersity and negative charge are key modulators of extracellular matrix deposition under macromolecular crowding conditions. Acta Biomaterialia. 2019 Apr;88:197–210. Available from: https://doi.org/10.1016/j.actbio.2019.02.050.

[113] Cavanzo NP, Bigaeva E, Boersema M, Olinga P, Bank RA. Macromolecular Crowding as a Tool to Screen Anti-fibrotic Drugs: The Scar-in-a-Jar System Revisited. Frontiers in Medicine. 2021 Jan;7. Available from: https://doi.org/10.3389/fmed.2020.615774.

[114] Cheng R, Zhang F, Li M, Wo X, Su YW, Wang W. Influence of Fixation and Permeabilization on the Mass Density of Single Cells: A Surface Plasmon Resonance Imaging Study. Frontiers in Chemistry. 2019 Aug;7. Available from: https://doi.org/10.3389/fchem.2019.00588.

[115] Baum J, Duffy HS. Fibroblasts and Myofibroblasts: What Are We Talking About? Journal of Cardiovascular Pharmacology. 2011 Apr;57(4):376–379. Available from: https://doi.org/10.1097/fjc.0b013e3182116e39.

[116] Qureshi OS, Bon H, Twomey B, Holdsworth G, Ford K, Bergin M, et al. An immunofluorescence assay for extracellular matrix components highlights the role of epithelial cells in producing a stable, fibrillar extracellular matrix. Biology Open. 2017 Oct;6(10):1423–1433. Available from: https://doi.org/10.1242/bio.025866.

[117] Hobro AJ, Smith NI. An evaluation of fixation methods: Spatial and compositional cellular changes observed by Raman imaging. Vibrational Spectroscopy. 2017 Jul;91:31–45. Available from: https://doi.org/10.1016/j.vibspec.2016.10.012.

[118] Kang H, Rho S, Stiles WR, Hu S, Baek Y, Hwang DW, et al. Size-Dependent EPR Effect of Polymeric Nanoparticles on Tumor Targeting. Advanced Healthcare Materials. 2019 Dec;9(1):1901223. Available from: https://doi.org/10.1002/adhm.201901223.

[119] Lammers T, Kiessling F, Hennink WE, Storm G. Drug targeting to tumors: Principles, pitfalls and (pre-) clinical progress. Journal of Controlled Release. 2012 Jul;161(2):175–187. Available from: https://doi.org/10.1016/j.jconrel.2011.09.063.

[120] Xia Y, Sun J, Liang D. Aggregation, Fusion, and Leakage of Liposomes Induced by Peptides. Langmuir. 2014 Jun;30(25):7334–7342. Available from: https://doi.org/10.1021/la501618f.

[121] Shao XR, Wei XQ, Song X, Hao LY, Cai XX, Zhang ZR, et al. Independent effect of polymeric nanoparticle zeta potential/surface charge, on their cytotoxicity and affinity to cells. Cell Proliferation. 2015 May;48(4):465–474. Available from: https://doi.org/10.1111/cpr.12192.

[122] Gong H, Holcomb I, Ooi A, Wang X, Majonis D, Unger MA, et al. Simple Method To Prepare Oligonucleotide-Conjugated Antibodies and Its Application in Multiplex Protein Detection in Single Cells. Bioconjugate Chemistry. 2016 Jan;27(1):217–225. Available from: https://doi.org/10.1021/acs.bioconjchem.5b00613.

[123] Gai M, Simon J, Lieberwirth I, Mailänder V, Morsbach S, Landfester K. A bio-orthogonal functionalization strategy for site-specific coupling of antibodies on vesicle surfaces after self-assembly. Polymer Chemistry. 2020;11(2):527–540. Available from: https://doi.org/10.1039/c9py01136f.

[124] Simonian MH. Spectrophotometric Determination of Protein Concentration. Current Protocols in Food Analytical Chemistry. 2002 May;4(1). Available from: https://doi.org/10.1002/0471142913.fab0103s04.

[125] Saraiva MA. Interpretation of -synuclein UV absorption spectra in the peptide bond and the aromatic regions. Journal of Photochemistry and Photobiology B: Biology. 2020 Nov;212:112022. Available from: https://doi.org/10.1016/j.jphotobiol.2020.112022.

[126] Kuninty PR, Bansal R, Geus SWLD, Mardhian DF, Schnittert J, van Baarlen J, et al. ITGA5 inhibition in pancreatic stellate cells attenuates desmoplasia and potentiates efficacy of chemotherapy in pancreatic cancer. Science Advances. 2019 Sep;5(9). Available from: https://doi.org/10.1126/sciadv.aax2770.

[127] Hollett JW, Kelly A, Poirier RA. Quantum Mechanical Size and Steric Hindrance. The Journal of Physical Chemistry A. 2006 Dec;110(51):13884–13888. Available from: https://doi.org/10.1021/jp066011h.

[128] Grinnell F, Bennett MH. Fibroblast adhesion on collagen substrata in the presence and absence of plasma fibronectin. Journal of Cell Science. 1981 Apr;48(1):19–34. Available from: https://doi.org/10.1242/jcs.48.1.19.

[129] Croce MA, Silvestri C, Guerra D, Carnevali E, Boraldi F, Tiozzo R, et al. Adhesion and Proliferation of Human Dermal Fibroblasts on Collagen Matrix. Journal of Biomaterials Applications. 2004 Jan;18(3):209–222. Available from: https://doi.org/10.1177/0885328204039692.

[130] Shimizu K, Kobayashi M, Tahara J, Shiratori K. Cytokines and Peroxisome Proliferator-Activated Receptor Ligand Regulate Phagocytosis by Pancreatic Stellate Cells. Gastroenterology. 2005 Jun;128(7):2105–2118. Available from: https://doi.org/10.1053/j.gastro.2005.03.025.

[131] Guidelines for the use of flow cytometry and cell sorting in immunological studies. European Journal of Immunology. 2017 Oct;47(10):1584–1797. Available from: https://doi.org/10.1002/eji.201646632.

[132] Jiang JX, Chen X, Hsu DK, Baghy K, Serizawa N, Scott F, et al. Galectin-3 modulates phagocytosis-induced stellate cell activation and liver fibrosis in vivo. American Journal of Physiology-Gastrointestinal and Liver Physiology. 2012 Feb;302(4):G439–G446. Available from: https://doi.org/10.1152/ajpgi.00257.2011.

[133] Zhan SS, Jiang JX, Wu J, Halsted C, Friedman SL, Zern MA, et al. Phagocytosis of apoptotic bodies by hepatic stellate cells induces NADPH oxidase and is associated with liver fibrosisin vivo. Hepatology. 2006 Mar;43(3):435–443. Available from: https://doi.org/10.1002/hep.21093.

[134] Jesnowski R, Fürst D, Ringel J, Chen Y, Schrödel A, Kleeff J, et al. Immortalization of pancreatic stellate cells as an in vitro model of pancreatic fibrosis: deactivation is induced by matrigel and N-acetylcysteine. Laboratory Investigation. 2005 Aug;85(10):1276–1291. Available from: https://doi.org/10.1038/labinvest.3700329.

[135] McKleroy W, Lee TH, Atabai K. Always cleave up your mess: targeting collagen degradation to treat tissue fibrosis. American Journal of Physiology-Lung Cellular and Molecular Physiology. 2013 Jun;304(11):L709–L721. Available from: https://doi.org/10.1152/ajplung.00418.2012.

[136] Joo SH. Cyclic Peptides as Therapeutic Agents and Biochemical Tools. Biomolecules and Therapeutics. 2012 Jan;20(1):19–26. Available from: https://doi.org/10.4062/biomolther.2012.20.1.019.

[137] Rezvantalab S, Drude NI, Moraveji MK, Güvener N, Koons EK, Shi Y, et al. PLGA-Based Nanoparticles in Cancer Treatment. Frontiers in Pharmacology. 2018 Nov;9. Available from: https://doi.org/10.3389/fphar.2018.01260.

[138] Heinrich MA, Mostafa AMRH, Morton JP, Hawinkels LJAC, Prakash J. Translating complexity and heterogeneity of pancreatic tumor: 3D in vitro to in vivo models. Advanced Drug Delivery Reviews. 2021 Jul;174:265–293. Available from: https://doi.org/10.1016/j.addr.2021.04.018.

[139] Rodrigues J, Heinrich MA, Teixeira LM, Prakash J. 3D In Vitro Model (R)evolution: Unveiling Tumor–Stroma Interactions. Trends in Cancer. 2021 Mar;7(3):249–264. Available from: https://doi.org/10.1016/j.trecan.2020.10.009.

A Appendix

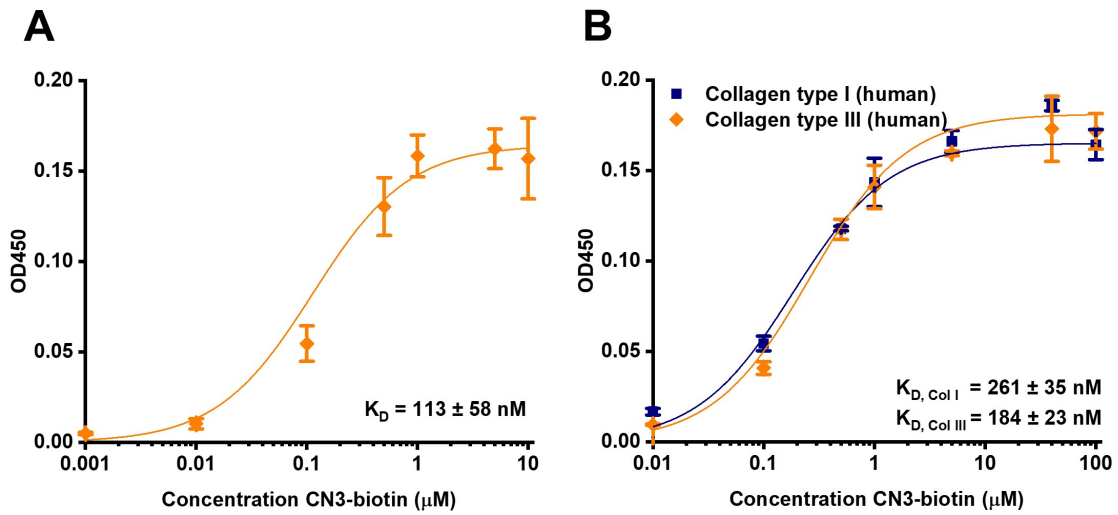

Figure A1: CN3-biotin binding experiments using ELISAs . A) Estimated binding affinity of CN3-biotin to collagen type III (n=6, 3 experimental replicates). B) Comparison between human collagen types I and III using few methodical alterations, as described in the results section (n=3).

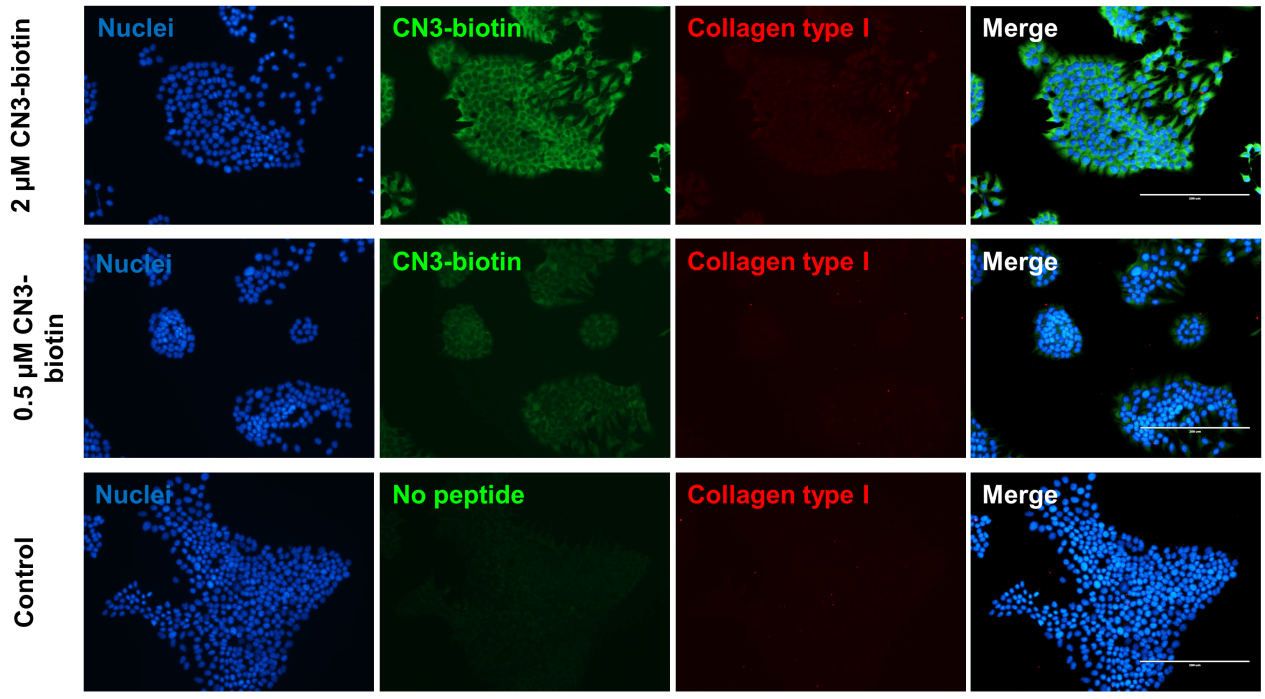

Figure A2: Immunofluorescence of KPC cells. KPC cells were stained with 4′,6-diamidino-2-phenylindole (DAPI, blue), CN3-biotin (green), and goat anti-collagen type I (red). CN3-biotin was used at 2 μM, 0.5 μM, and 0 μM. Representative images (n=3), scale bar = 200 μm.

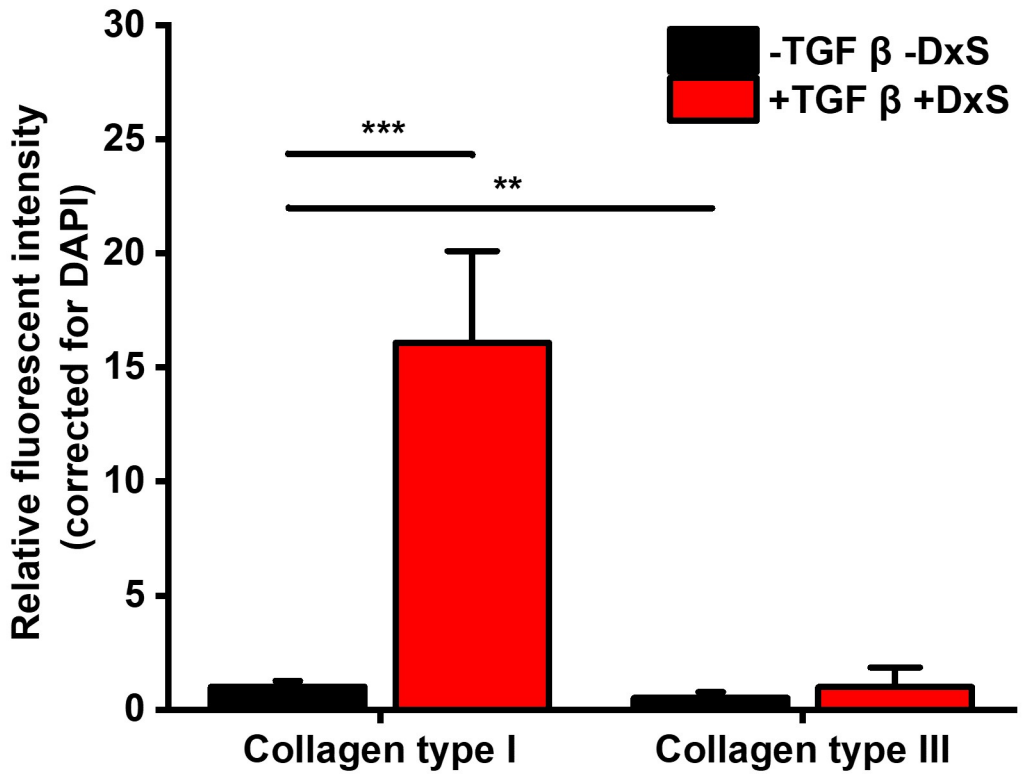

Figure A3: Quantification of collagen deposition for collagen type I and collagen type III with or without TGF-β1 and Dextran Sulfate >500 kDa (n=6). Statistical analyses were done using analysis of variance (ANOVA). $**p<0.01$; $***p<0.001$.

Table A1: Lipid molar ratio (HSPC, Cholesterol, Lipoid PE 18:0/18:0-PEG 2000, and DSPE-PEG-DBCO) and the extrusion protocol tested that lead to the final formulation. ∗*Extrusion and new collection tube on the next day*

Lipid molar ratio	**Extrusion filter (pore size in μm)**	**Extrusion repetitions**	**Size (nm) (n=3)**	**PDI (n=3)**	**Remarks**
7.5:2:0.25:0.25	0.4 + 0.4 0.2 + 0.2 0.1 + 0.1	3 3 6	171 ± 2	0.24 ± 0.02	Sedimentation when stored at 4°C
7.5:2:0.4:0.1	0.4 + 0.4 0.2 + 0.2 0.1 + 0.1	3 3 8	133 ± 2	0.13 ± 0.02	
6.5:3:0.4:0.1	0.4 + 0.4 0.2 + 0.2 0.1 + 0.1	3 3 12	142 ± 1	0.12 ± 0.01	30 mol% cholesterol for more stable particles
6.5:3:0.4:0.1	0.4 + 0.4 0.2 + 0.2 0.1 + 0.1 0.08 + 0.08*	3 3 3 5	125 ± 1	0.10 ± 0.02	
6.5:3:0.4:0.1	0.4 + 0.4 0.2 + 0.2 0.1 + 0.1 0.08 + 0.08 0.05 + 0.05*	3 3 3 5 5	114 ± 1	0.20 ± 0.01	
6.5:3:0.4:0.1	0.4 + 0.4 0.2 + 0.2 0.1 + 0.1 0.08 + 0.08 0.08 + 0.05* 0.05 + 0.05*	3 3 3 10 3 4	92 ± 1	0.13 ± 0.01	
6.5:3:0.4:0.1	0.4 + 0.4 0.2 + 0.2 0.1 + 0.1 0.08 + 0.08	3 3 3 10	98 ± 0	0.10 ± 0.01	New collection tube after extrusion 0.1 μm filters

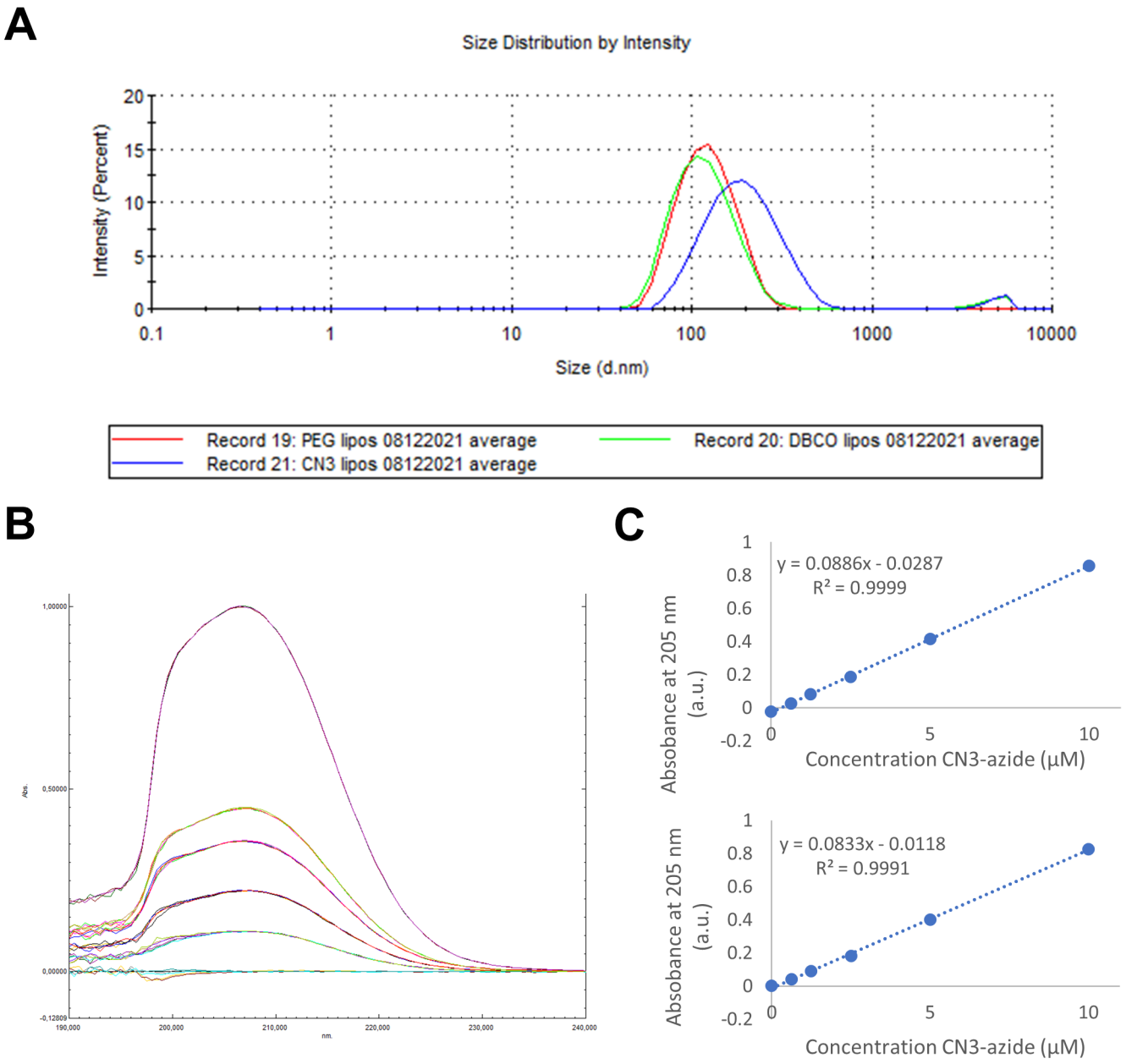

Figure A4: Raw data on liposome size and absorbance of CN3-peptide. A) Size distribution intensities as measured by the Malvern ZetaSizer (n=3, representative distributions shown). B) Absorbance per wavelength (nm) of different concentrations CN3-azide as measured on the Shimadzu spectrophotometer. Strong absorbance can be observed around 205 nm. C) Calibration curves used to calculate the coupling-efficiency of CN3-azide to the DBCO-liposomes.